AMERICAN UNIVERSITY OF BEIRUT

HYDROTHERMAL CARBONIZATION OF OLIVE OIL MILL WASTE WATER

by
EMILE ELIA ATALLAH

A thesis
submitted in partial fulfillment of the requirements
for the degree of Master of Chemical Engineering
to the Department of Chemical and Petroleum Engineering
of the Maroun Semaan Faculty of Engineering and Architecture
at the American University of Beirut

Beirut Lebanon
April 2018

AMERICAN UNIVERSITY OF BEIRUT

HYDROTHERMAL CARBONIZATION OF OLIVE OIL MILL WASTE WATER

by
EMILE ATALLAH

Approved by:

Joseph Zeaiter

Dr. Joseph Zeaiter, Associate Professor
Department of Chemical and Petroleum Engineering
Advisor

Walid Saad
On behalf of

Dr. Mohammad Ahmad, Professor, Chairman
Department of Chemical and Petroleum Engineering
Member of Committee

Dr. Mu'Tasem Shehadeh, Associate Professor,
Department of Mechanical Engineering
Member of Committee

Date of thesis defense: April 26, 2018

AMERICAN UNIVERSITY OF BEIRUT

THESIS, DISSERTATION, PROJECT RELEASE FORM

Student Name:_____Atallah___________________Emile______________Elia____
Last First Middle

● Master's Thesis ○ Master's Project ○ Doctoral Dissertation

☐ I authorize the American University of Beirut to: (a) reproduce hard or electronic copies of my thesis, dissertation, or project; (b) include such copies in the archives and digital repositories of the University; and (c) make freely available such copies to third parties for research or educational purposes.

☑ I authorize the American University of Beirut, to: (a) reproduce hard or electronic copies of it; (b) include such copies in the archives and digital repositories of the University; and (c) make freely available such copies to third parties for research or educational purposes after:

One ---- year from the date of submission of my thesis.
Two ---- years from the date of submission of my thesis.
Three --✓-- years from the date of submission of my thesis.

Emile May 10, 2018
Signature Date

ACKNOWLEDGMENTS

This work was financially supported by the university research board at AUB (URB) and the Munib and Angela Masri Institute for Energy and Water Resources.

AN ABSTRACT OF THE THESIS OF

Emile Atallah for Master of Science

Major: Chemical Engineering

Title: Hydrothermal Carbonization of Olive Oil Mill Waste Water

Hydrothermal carbonization (HTC) is an emerging technique for wastewater treatment. It uses water at moderate temperatures (180-250℃) and autogenous pressures (35-55 bar) to break down organic waste. In this work, HTC was used to treat olive oil mill wastewater. The reaction time and the water-sludge (W/S) ratio were varied, over a broad set of values, to study their effect on the hydrochar products.
As the reaction time and dilution factor increased, the hydrochar conversion was low and decreased from 36 % to 7 % while the liquid product mass was always high and increased from 93.5 g to 176.5 g. HTC upgraded both carbon and energy content to very high values, 72 % and 36 MJ/Kg respectively. Hence, the produced hydrochar is a good candidate for energy production. Besides, the produced hydrochars were amorphous and had a hydrophobic structure due to their phenolic and acidic content. Their filament structure became apparent and more evident as the dilution factor increased. Hydrochar yield was the highest at the lowest dilution factor (i.e. 1.5) and reaction time (2 hours), while carbon percentage and calorific values were significantly high and not affected by the change in the operating conditions. The Sulfur level was always negligible while chlorine level reached approximately zero at higher operating condition.

Liquid extracts were taken under various operating conditions, and different analytical techniques were used to analyze the acids/phenols quality and concentrations along with the non-polar hydrocarbons in the liquid phase. Different extraction methods were developed and tested in this work along with GC-MS and UV analyses. Many simple biophenols such as Tyrosol, hydroxyl-Tyrosol, phenol, homo-vanillyl alcohol, along with various ketones, flavones, flavonols, alcohol, aldehydes, cyclic/aromatics, alkanes, alkenes and even alkynes were detected in the liquid phase product. In contrast, negligible amounts of polyaromatic hydrocarbons (PAH) were found. The hydrocarbons concentration decreased as the reaction time and water to sludge ratio were increased. A detailed ultraviolet quantification method was developed and showed that the total acids/phenols content decreased 10 folds when the water to sludge ratio increased by a factor of 9 under a reaction time of 8 h. Alternatively, optimum HTC conditions were found to be at a 3.5 dilution factor and 4 h reaction time.

Keywords: Hydrothermal carbonization, Hydrochars, Liquid Phase Analysis, Phenols, Acids, Hydrocarbons, characterization

CONTENTS

Chapter

ILLUSTRATIONS

TABLES

Table Page

CHAPTER I

INTRODUCTION

The Mediterranean countries are famous for their olive trees. Some of the olive beans are used in daily food production. However, the most significant quantity is put in the olive press, where under high pressure, the olive seeds are squeezed, and all the rich liquid oil is taken out. This liquid is then driven to a filter where it is separated between pure olive oil and olive oil mill waste (OOMW). In most of the Mediterranean countries, due to the absence of a waste plan, water is added to this waste to dilute it, then it is disposed of in the sewage system or in nature (lakes, rivers, etc.).

The olive oil mill wastewater is extremely dangerous for the aquatic life. Out of the total olive oil mill output, OOMW (by volume) accounts for up to 50 %, while the olive oil accounts for 20 % and the remaining 30 % is the solid residue known in Lebanon as Jift [1]. Over 7.3 million tons per year (t/y) of OOMW is generated worldwide, originating from the extraction of around 1.825 million tons per year of olive oil from 9.7 million tons of olives [2]. Many studies describe OOMW as a significant pollutant to surface and groundwater resources in the Mediterranean basin since it has a very low biodegradable natural compound. This is mainly due to its high phytotoxic phenolic content, colored organic substances, and high organic matter concentration [3-5]. Besides, OOMW has a strong phytotoxic smell due to its antimicrobial activity [6, 7]. General approximated constituents of the OOMW are established in Table 1 where each one has a negative environmental impact if disposed of without treatment, with the phenolic OOMW being the most polluting constituents

[8]. The Biological Oxygen Demand (BOD) of the OOMW can reach values as high as 70,000 ppm (100,000 mg/l) and the Chemical Oxygen Demand (COD) around 200,000 ppm (200,000 mg/l) [9]. OOMW environmental problems do not just affect water, but it also has some phytotoxic effects especially on plants germination and early fall of the fruit and vegetable senescence [2].

Table 1: Characteristics and composition of OMW[1, 10, 11]

OMW characteristic	Value
Color	Intensive violet-dark brown up to black
Odor	Strong specific olive oil smell, fetid smell
pH	4.5 - 6.0
Water Content	83 - 92 %
Organic and Volatile Material	7 - 15 %
Mineral Solids	1 - 2 %
Residual Oil	0.3 - 10.0 %
Total Sugars	2 - 8 %
Reducing Sugars	1 - 8 %
Polyalcohol	1.0 - 1.5 %
Protein	0.5 - 7.5 %
Pectin and Tannins	1.0 - 1.5 %
Phenols	17 %
Suspended Solids	5,000 – 35,000 ppm
BOD_5	65,000 – 70,000 ppm
COD	40,000 – 200,000 ppm

OOMW has a dark liquid effluent color. It is characterized by its high concentration of organic compounds, including organic acids, sugars, tannins, pectin and phenolic substances that make the waste phytotoxic and inhibit bacterial activity [12]. Consequently, OOMW takes a long time to degrade when disposed of in nature.

Regarding pollution, one cubic meter of OOMW is equivalent to 100–200 cubic meters of domestic sewage, which is very high from a waste treatment perspective. It is widely disposed of in water reservoirs in an uncontrolled manner. This causes severe problems for the entire discipline of the ecosystem [12].

The main problem in OOMW treatment is that its composition is highly dependable on the cultivation environment, harvesting time and oil extraction technology. Thus, its composition is going to vary from time to time and from place to another. Hence, a general characterization of the OOMW is almost absent. This makes the treatment process more challenging.

There are several ways to treat OOMW, but each one has its own disadvantages with respect to toxicity, low recovery, high capital cost, etc. After adding specific materials to it, it can be used as a fertilizer to help the soil and enhance the microbial growth. However, it has phytotoxic effects if it is used directly on the land. Some researchers claim that it can be used for particular animal feed, but it will cause antidigestive problems. It can be used in the recovery process of antioxidants and enzymes mainly because it contains several water-soluble compounds, but the recovery is associated with high cost. It can help in the production of alcohols since it contains sugars, but the fermentation yeast yield is low, same problem when using it in biopolymers production. In addition, it can be used as a feed stream in the anaerobic degradation process of methane, but it is highly toxic [13].

Another solution to the problem is to use Fenton agent which degrades all the organic materials and purify the waste. In addition, previous researchers suggested using oxygen-consuming microorganisms such as bacteria to eliminate the organic compounds in the waste [14]. However, these two processes are not economically feasible.

In Di Lecce's study, OOMW was treated using membranes that represent promising technologies for the recovery of water, organic compounds, and antioxidants from OOMW. This technique has several advantages in terms of low energy consumption, no additives requirement, and no phase change. An integrated membrane system working at two different concentration factors was used. The effect of two membrane-based filtration steps (microfiltration and nanofiltration) on the content of chemical oxygen demand, dry matter, visual quality, phenolic compounds and antioxidant activity of permeate and retained samples were also studied and evaluated. The results showed a noticeable decrease in the COD and phenolic content, but at high cost [15].

A unique characteristic of OOMW is its calorific value that is similar to wood or soft coal (lignite). In addition, it has similar density, general burning characteristics, lower emissions, and higher efficiency than natural coal. As a result, olive residues and coal act as compatible co-combustion materials. Hence, OOMW can be used as a better coal replacement in waste to energy processes. However, for gasification, it requires massive capital cost and highly qualified personals due to the complication and environmental impacts of the gasification process. On the other hand, in combustion, OOMW needs another form of energy to be burnt and can cause several problems in the process especially if a fluidized bed is used. Torrefaction can also be used, and it has a low energy requirement, but the wet biomass needs to be actively dried before using it which adds significant evaporation cost. As a result, a new waste to energy process is introduced in this work which is hydrothermal carbonization.

Hydrothermal carbonization (HTC) is a process that uses just water at a relatively low temperature, between 180℃ and 250℃, to degrade the OOMW and produce a solid product, known as hydro-char. HTC reaction lowers the oxygen and hydrogen content in the raw material mainly due to the dehydration and decarboxylation reactions happening at high temperature in aqueous medium [16]. The produced char is a bituminous coal like material that is stable, non-toxic [16, 17], and can be used as an energy source, for soil amelioration, and as a sorbent in water treatment processes [17]. The products characteristics, their relative gas/liquid/solid proportions, and the energy content depend on the raw materials used and operating conditions. The main advantage of the HTC reaction is that it can convert low energetic and wet materials into carbonaceous solid with high carbon yield and high energy content. HTC has a relatively low cost due the low temperature/energy requirements and the absence of any intensive energy drying before or during the process [17]. Hence, several researchers tried to study the effect of temperature, and reaction time on the produced hydrochars.

Olive oil derivatives have been for a long time a center for study in hydrothermal carbonization. Lopez et al. studied the effects of temperature and reaction time on the furfural production from the hydrothermal carbonization process of the olive stones. They presented a thorough qualification and quantification of their liquid products[18]. Volpe et al. studied the effect of temperature and solid to water ratio on the secondary char formations of the olive trims and olive pulps. They have found that the higher the solid to water ratio, the higher were the degree of carbonization, the hydrochar heating values (HHV), and the hydrochar yield. Besides, high solid load and high temperature promoted secondary char formation that has higher carbon content and hence higher energy [19].

Benavente el al. studied the effect of temperature and reaction time on the hydrochar products from hydrothermal carbonization of olive oil mill waste (OOMW). They have found that as the reaction time and temperature increase, moisture content and hydrochars yield decrease while the carbon content increases. Furthermore, sulfur decreased while Si, Mg, P, Fe, and Cl all increased with increasing reaction time and temperature. In addition, they compared between the energy usage of HTC and that of torrefaction, and found a 50% more savings when using HTC [20].

The reaction mechanisms highly dominate the feedstock decomposition. It is well known that five reactions govern HTC. These are hydrolysis, dehydration, decarboxylation, aromatization, and recondensation [16, 17]. Hydrothermal carbonization is initiated by hydrolysis which makes the initial raw material less stable under hydrothermal conditions which lower the decomposition temperature [17]. As a result, Hemicellulose decomposes between 180℃ and 200^{0}C, most of the lignin between 180℃ and 220℃, and cellulose above 220℃ [17]. Lignin degrades into simple phenols, ketones, acids, and aldehydes [21]. As the reaction time increases, more degradation takes place. On the other hand, water acts as both solvent and catalyst in the degradation process. Hence, increasing the dilution factor will lead to more degradation of the organic phase, followed by diffusion to the liquid phase.

Furthermore, HTC reaction has the capability to significantly decrease the alkali metals concentration and most of the inorganic materials, which are found in a significant quantity in the raw materials, to a very low level [17, 20, 22]. This is mainly due to hemicellulose removal at an operating temperature higher than 180℃ [22].

The high-water content in OOMW makes HTC a perfect candidate for the treatment process. In addition, the low temperature operation of the HTC process is very important economically. Furthermore, the nature of HTC products, that can be used as a source of energy, makes it one of the best candidates to solve this problem.

However, the liquid product has a high acids and phenols contents[1, 4, 5, 7, 13, 16, 19, 20, 23-26]. This liquid product is undesirable due to the fact that many organic material and valuable carbon in the solid products will dissolve into the liquid part[25]. In addition, the increase in degradation level which will increase the phenolic content in the liquid products causes a huge disposal problem due to its low biodegradability and high toxicity for the whole ecological system.

According to several studies, phenolic contents from olive oil have several health benefits. They have some cancer chemoprevention, cardioprotective, and neuroprotective activities[24, 27]. In addition, some epidemiology studies correlate the low occurrence of heart diseases and cancers to the high olive oil consumption in the Mediterranean diet[24, 28]. Hence, natural phenols from olive oil and olive oil wastewater can be a good potential for food, cosmetics, soap, and pharmaceutical industries[24].

According to previous researchers, a wide variety of organic compounds could be identified in the aqueous HTC solution. Aromatic alcohol such as OH-Tyr, Tyr, and homovanillic alcohol were found abundantly in the solution[25, 26, 28]. Benzoic acids and derivatives, cinnamic acids, phenyl ethyl alcohols, phenolic acids, flavonols, lignans, isochromans, and secoiridoids could all be found in the solution too[25, 26, 28]. All these compounds are derived from the degradation of cellulose, hemicellulose, and especially lignin that is found abundantly in the OOMW initial solution[7, 24, 25]. A large list of underivatized analytes, aromatic and aliphatic acids, aliphatic and aromatic alcohols, nitrogen and sulfur compounds, monosaccharides, and phenols is shown in the work of Poerschmann, both in the olive oil mill wastewater and the liquid phase[25, 26].

On the other hand, polycyclic aromatic hydrocarbons (PAH) are organic compounds containing two or more fused aromatic rings made up of carbon and hydrogen atoms[29]. They are considered as ubiquitous environmental contaminants that are highly mutagenic and carcinogenic. They are usually formed and released during incomplete combustion, by industrial processes, and as a result of an anthropogenic activity[30]. PAH formation depends on the type and composition of the raw materials, oxygen accessibility, temperature, and time[29].

The occurrence of PAH in vegetable oil, such as olive oil, is mostly related to their thermal treatment. As a result, the oil and fats in the raw material, due to their high lipophilic nature and lignin content, will degrade into PAH. While many studies reported the existence of 16 PAH, 8 of them which are benzo[a]anthracene, chrysene, benzo[b]fluoran-thene, benzo[k]fluoranthene, benzo[a]pyrene, indeno[1,2,3-c,d]pyrene, di-benzo[a,h]anthracene and benzo[g,h,i]perylene are considered to be the most carcinogenic PAH[29-31].

CHAPTER II

AIM OF THE PROJECT

To our knowledge, several researchers investigated the temperature effect on HTC process, and found that the degree of carbonization increases with the increase in temperature. However, very little research was conducted on the influence of reaction time and water-sludge ratio (dilution factor) on the produced hydrochar quality and properties. Although many researchers think that water-sludge ratio is the least important, this study shows that dilution factor is highly important and can lead to an optimized condition for hydrochar formation. Hence, HTC experiments were carried out at different reaction times (2h, 4h, and 8h) with a varying water-sludge ratio from 1.5 up to 9. A full characterization of the hydrochars at each operating condition is shown in this study.

In addition, a quantitative and qualitative analysis for the phenolic, acidic, and polyaromatic hydrocarbons in each condition was conducted. The main aim was to test the effect of the water-sludge ratio and reaction time on reducing the phenolic-acids and PAH contents in the final liquid product.

CHAPTER III

EXPERIMENTAL SECTION

A. Materials

Fresh olive oil mill waste was supplied by a local supplier. Usually, high quantity of water is added to the OOMW before it is disposed of in the sewage. Hence, the water content in the fresh raw materials was around 80%. As a result, the raw material was dried on an MSH-20D WiseStir heater equipped with a stirrer at 60℃ for around 73 hours until reaching a water content of around 7% below which the OOMW started to oxidize. Pure ethyl acetate, acetone and hexane (according to each method) was used for extraction before GC-MS liquid phase analysis. Folin-Ciocalteu reagent 0.2 N (Sigma-Aldrich) was also used as color indicator for the phenols-acids quantification while pure powder Gallic acid (Sigma-Aldrich) was used as internal standard.

B. HTC experimental procedure

The experiments were carried out in an 0.5 L, electrically heated, high pressure Parr reactor. In each experiment, only water was added to the sludge (dried OOMW) inside the reactor according to the water to sludge ratio. Then, the reactor was closed and sealed without nitrogen purge. The reactor pressure was not controlled in the experiments and was kept autogenic with the vapor pressure of water at the setpoint temperature. However, in all experiments, the pressure was reaching around 50 bar at 250℃. Measurements of the reaction time began when the reactor reached the HTC operating temperature. After completing each experiment, the reactor was immersed in a cold bath to cool down the apparatus and stop the reaction. Then, its pressure valve was opened to release all gases and any pressure build-up inside. The gas was not collected since its analysis is out of scope. A vacuum pump along with a DP 400 110 filter paper were used to separate the remaining solid-liquid mixture. The mass of both solid and liquid products was measured, then each was stored in a well-sealed sample holder at 4℃ prior to any further analysis. All experiments were repeated three times and the results were averaged in each case and summarized in Table 2 below.

Table 2: Reaction products yield

				Products (%)			
	Water (g)	**Sludge (g)**	**Total (g)**	**Gas***	**Liquid**	**Solid**	**Yield** (%)**
OMW 2H - W/S = 1.5	75	50	125	10.64	74.80	14.56	36.4
OMW 2H - W/S = 2.5	125	50	175	8.74	83.43	7.83	27.4
OMW 2H - W/S = 3.5	175	50	225	12.67	81.60	5.73	25.8
OMW 2H - W/S = 5	250	50	300	16.70	82.23	1.07	6.4
OMW 2H - W/S = 7	350	50	400	11.88	87.23	0.90	7.2
OMW 2H - W/S = 9	180	20	200	20.95	78.15	0.90	9
OMW 4H - W/S = 1.5	75	50	125	11.20	74.80	14.00	35
OMW 4H - W/S = 2.5	125	50	175	9.31	84.06	6.63	23.2
OMW 4H - W/S = 3.5	175	50	225	20.04	78.44	1.51	6.8
OMW 8H - W/S = 3.5	175	50	225	20.13	78.44	1.42	6.4
OMW 8H - W/S = 9	180	20	200	25.10	74.00	0.90	9

* calculated as a difference

** Yield = dry solid / dry sludge

C. Hydrochar analysis methods

Samples from each solid product were analyzed after separation. A Bruker X-Ray Diffraction (XRD) machine was used to check for any crystal structure inside the solid samples. A Scanning Electron Microscope (SEM MIRA 3 LMU Tescan, Czech Republic) and the software for image analysis of the micrographs (Tescan Software, Czech Republic) were used to show the structure of the solid samples and to evaluate the ash and minerals compositions. Each EDX value was repeated three times and the average was taken. It should be noted that the repeated analysis values did not show much discrepancy. CHNS elemental analyzer was also used to evaluate the ultimate analysis. Oxygen percentage was calculated by subtracting the carbon, hydrogen, nitrogen, and ash percentages from the total percentage. The results are all shown in Table 3. O/C and H/C ratios were calculated and shown in Table 4 and are plotted in Figure 2 in Van Krevelen diagram for the solid fuel production.

Table 3: Ultimate analysis, and ash and minerals contents (on a wet basis)

Sample name	**C %**	**H %**	**N %**	**O %**	**Ash content**	**Mg %**	**Al %**	**P %**	**Ca %**	**K %**	**Cl %**	**S %**
OMW 2H - W/S = 1.5	72.37	9.91	2.05	10.74	4.93	0.48	0.19	1.12	2.17	0.75	0.22	less than 0.1%
OMW 2H - W/S = 2.5	72.24	9.97	1.81	11.06	4.92	0.25	0.04	1.03	1.41	1.65	0.54	less than 0.1%
OMW 2H - W/S = 3.5	73.45	10.61	1.62	8.39	5.93	1.21	0.04	1.76	1.98	0.76	0.18	less than 0.1%
OMW 2H - W/S = 5	73.35	10.7	1.59	8.27	6.09	0.77	0.03	1.76	3.15	0.32	0.06	less than 0.1%
OMW 2H - W/S = 7	73.23	10.57	1.4	9.91	4.89	0.49	0.01	1.41	2.81	0.15	0.02	less than 0.1%
OMW 2H - W/S = 9	72.33	10.36	1.56	14.26	1.49	0.18	0.07	0.47	0.71	0.05	0.01	less than 0.1%

OMW 4H - W/S = 1.5	73.38	10.04	1.91	10.34	4.33	0.18	0.34	1.48	1.36	0.73	0.24	less than 0.1%
OMW 4H - W/S = 2.5	72.54	9.93	1.82	11.13	4.58	0.28	0.28	0.4	2.7	0.74	0.18	less than 0.1%
OMW 4H - W/S = 3.5	70.05	9.56	1.78	14.53	4.08	0.27	0.11	1.55	1.89	0.21	0.05	less than 0.1%
OMW 8H - W/S = 3.5	72.77	10.11	1.8	5.8	9.52	1.27	0.55	2.42	4.71	0.5	0.07	less than 0.1%
OMW 8H - W/S = 9	73.63	9.85	1.84	6.78	7.9	0.87	0.34	2.78	3.67	0.22	0.02	less than 0.1%
Raw material	52.18	6.09	0.67	35.37	5.69	0.18	0.39	0.37	0.56	3.81	0.38	less than 0.1%

Table 4: O/C AND H/C (x10) ratios

Sample name	H/C	O/C
OMW 2H - W/S = 1.5	1.37	0.15
OMW 2H - W/S = 2.5	1.38	0.15
OMW 2H - W/S = 3.5	1.44	0.11
OMW 2H - W/S = 5	1.46	0.11
OMW 2H - W/S = 7	1.44	0.14
OMW 2H - W/S = 9	1.43	0.20
OMW 4H - W/S = 1.5	1.37	0.14
OMW 4H - W/S = 2.5	1.37	0.15
OMW 4H - W/S = 3.5	1.36	0.21
OMW 8H - W/S = 3.5	1.39	0.08
OMW 8H - W/S = 9	1.34	0.09
Raw material	1.17	0.68

The moisture content was calculated from the total loss of samples placed in an oven at 105°C according to the European standards EN 14774-3:2009. The ash content and the volatile matter were obtained using an oven, lids, and crucibles, according to the European standards EN 14775:2009 and EN 15148:2009 respectively. The fixed carbon content was calculated by subtracting the moisture content, volatile matter, and ash content, all together from the initial sample weight. Similarly, the bulk density was calculated according to the European standards BS EN 15103:2009. All the results are shown in Table 5 below.

Table 5: Proximate analysis (all in grams)

Sample name	Bulk density	Moisture	Volatile Matter	Ash content	Fixed carbon
OMW 2H - W/S = 1.5	0.54	25.69	62.58	4.93	6.80
OMW 2H - W/S = 2.5	0.63	17.80	71.96	4.92	5.32
OMW 2H - W/S = 3.5	0.56	23.05	68.92	5.93	2.10
OMW 2H - W/S = 5	0.38	26.79	66.23	6.09	0.89
OMW 2H - W/S = 7	0.34	29.13	64.78	4.89	1.20
OMW 2H - W/S = 9	0.02	64.73	33.59	1.49	0.18
OMW 4H - W/S = 1.5	0.41	19.23	66.90	4.34	9.54
OMW 4H - W/S = 2.5	0.59	13.09	75.48	4.59	6.85
OMW 4H - W/S = 3.5	0.67	16.52	73.29	4.08	6.11
OMW 8H - W/S = 3.5	0.99	20.73	65.37	9.52	4.38
OMW 8H - W/S = 9	0.17	44.39	47.20	7.91	0.51
Raw material	0.27	74.75	19.32	5.69	0.24

Spill or droplet losses when emptying the reactor and during the separation of the solid-liquid mixture product were assumed to be negligible. In addition, since the liquid phase consists of water and several organic materials, some of them might be retained inside the solid hydrochar. Hence, the composition of the volatile matter content of the hydrochars was evaluated using a NETZ5CH F1 LIBRA R Thermogravimetric Analyzer (TGA) equipped with a BRUKER OPTIK GmbH Tensor 27 Fourier-transform infrared spectroscopy (FTIR). TGA temperature was varied from

25℃ to 900℃ under nitrogen flow, and a best fit of each peak is shown in Figure 1 using the FTIR library.

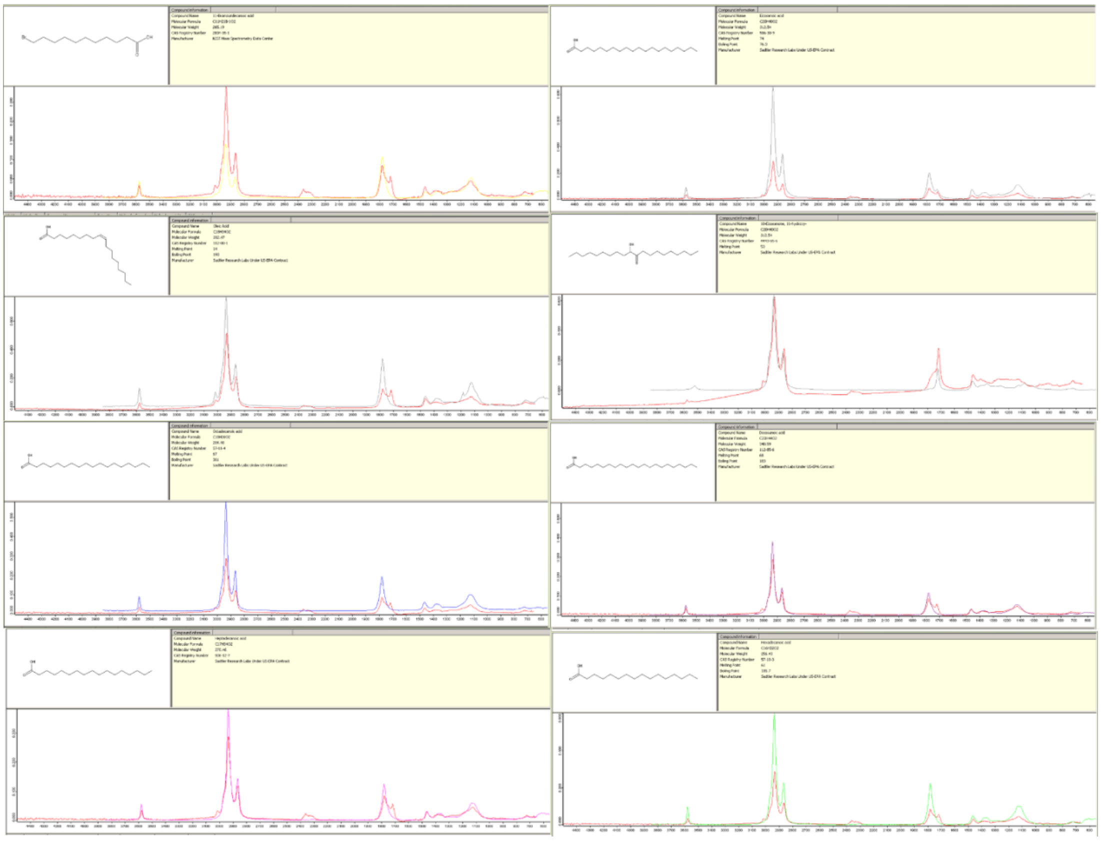

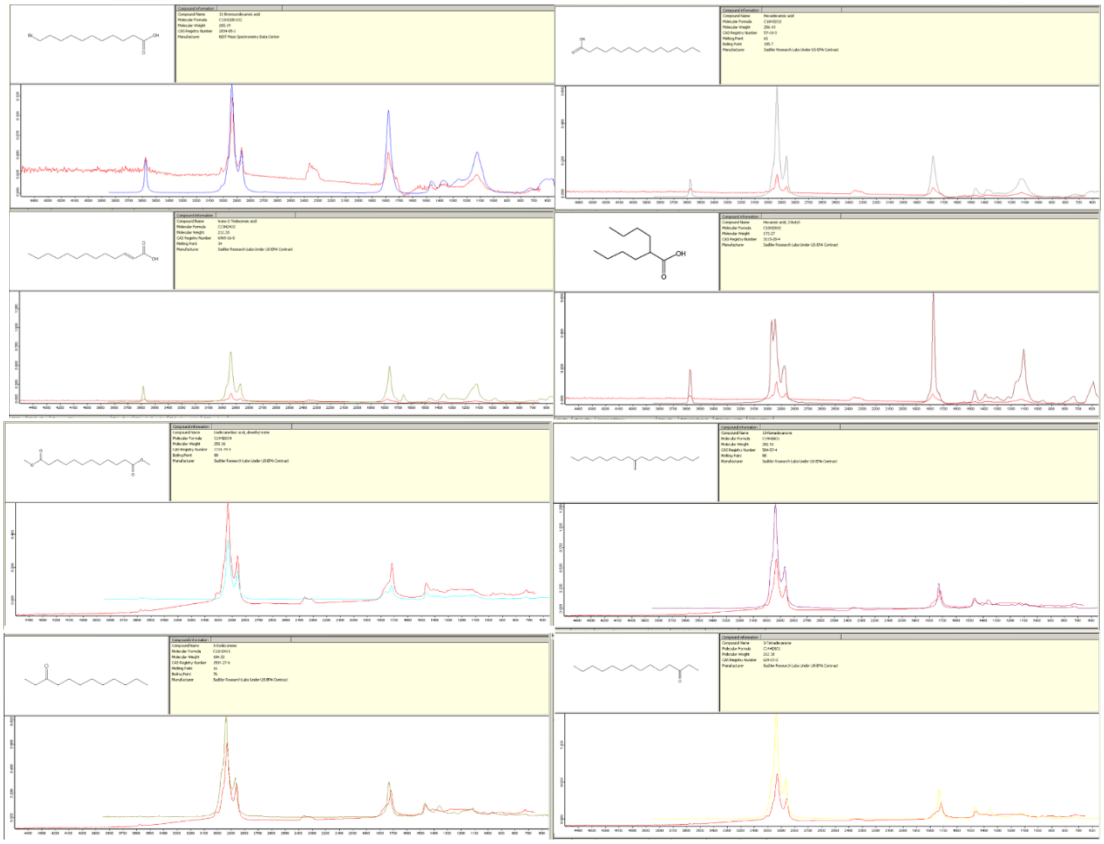

Figure 1: TGA-FTIR analysis results of the hydrochars

Brunauer–Emmett–Teller analysis (BET) was done after calcination of the hydrochar at 450℃ for 6 hours. The samples were degassed under vacuum pressure at 220℃ for 24 hours followed by BET analysis. The BET surface area was measured using QuantaChrome AS1Win™ - Autosorb 1 based with Micrometrics Gemini VII instrument on the isotherm of liquid nitrogen at 77.3K. The BET surface area was calculated from the adsorption branches in the relative pressure range of 0.05-0.30. The average pore size and the pore volume were calculated using BJH method.

All samples were dried in the oven at 55℃ for 24 hours, then the calorific values were determined using an IKA®C200bomb calorimeter.

Water contact angle measurements were carried out using the sessile drop technique (SDT) by a CAM 200 optical tensiometer (KSV Instruments) equipped with 30 fps camera (Imaging Source) operating at a frame interval of 0.16 ms. Liquid droplets with a typical volume of 10 µL were dispensed onto sample surfaces using a precision micropipette. Samples were affixed to glass slides using double-sided adhesive tape. Static contact angles were calculated using CAM 2008 software, when the droplet initially stabilised on the surface, typically within two seconds after dispensing.

Table 6: Contact angle (CA) measurement for OMW 2H - W/S = 5

	CA Left (degrees)	**CA Right (degrees)**	**Average CA (degrees)**
OMW 2H - W/S = 5	52.3	49.05	50.7
	55.57	56.33	56

D. Liquid phase analytical methods

1. Acids-Phenols Characterization

a. Solvent extraction

8 mL of each liquid sample were taken and acidified with a hydrochloric acid to reach pH 2. The solution was left for 1 h at room temperature. It was then centrifuged at 6000rpm for 20 min.

After centrifugation, the supernatant was extracted with 8 mL ethyl acetate (1:1 ratio) at room temperature for 24 h at 600 rpm, and then filtered using a pipette supported with a filter.

b. GC-MS analysis method

GC–MS analysis was performed using a 5975C GC MSD gas chromatograph mass spectrometry from Agilent Technologies equipped with an Agilent HP-5MS capillary column (30 m × 0.25 mm × 0.25 µm). The column temperature was initially held at 45 °C for 3 min, then programmed to 230 °C at a rate of 3 °C/min with a hold time of 10 min, from 230 to 280 °C at a rate of 20 °C min^{-1} and with a final hold time of 3 min. Helium was used as the carrier gas and the column head pressure maintained at 12 psi (83kPa). The injector and detector temperatures were maintained at 250 and 300 °C, respectively, and the injection volume was 1 µL in splitless mode. The interface temperature was held at 250 °C. Mass spectra were scanned from 30 *m*/*z* to 500 *m*/*z* at a rate of 1.5 scans/s. Electron impact ionization energy was 70 eV.

2. *Polyaromatic hydrocarbons characterization*

a. Solvent extraction

Several analysis methods were used to determine the concentration of polyaromatic hydrocarbons (PAH) in the samples. All these methods gave excellent results (referred below) but have not detected any PAHs in them. These methods include:

1. The euroanalysis method developed by sigma-Aldrich [32].
2. Another method developed by AB SCIEX Concord, Ontario (Canada); AB SCIEX Warrington (UK); Restek Corporation, Bellefonte, Pennsylvania (USA) [30].
3. The extraction method epa-3511[33].
4. Another extraction method developed by Anne Jurek, an application chemist in EST analytical Cincimnati, OH [34].
5. A method developed in China using liquid-liquid extraction [35].

The method developed by Haleyur et al. [36] was used to detect various non-polar compounds including PAHs. In this method, 5 different solvents were used: hexane, dichloromethane, acetone: hexane (1:1), acetone: dichloromethane (1:1), and chloroform: methanol (2:1). According to this method, acetone: hexane (1:1), acetone: dichloromethane (1:1), and chloroform: methanol (2:1) gave the best results. Hence, they were tried each aside by taking 15 mL of the solvent and adding 3 mL of sample. The mixture was vortexed for 10 minutes and centrifuged for 5 minutes at 4696 rpm. It was then filtered using a syringe equipped with a 0.2 □m filter. The permeate was centrifuged again for 5 minutes at 4696 rpm, and 50 □L of it were taken and added to 950 □L of hexane. The new mixture was centrifuged for 10 minutes and then injected in the GC-MS.

b. GC-MS analysis method

GC-MS analysis was performed using a 5975C GC MSD gas chromatograph mass spectrometry from Agilent Technologies equipped with an Agilent SLB-5ms capillary column (20 m × 0.18 mm × 0.18 μm). The column temperature was initially held at 50 °C for 1 min, then programmed to 325 °C at a rate of 20 °C/min with a hold time of 6 min. Helium was used as the carrier gas with a flow of 1.4 mL/min. The injector and detector temperatures were maintained at 325 and 325 °C, respectively, and the injection volume was 1 μL in splitless mode. The interface temperature was held at 325 °C. Mass spectra were scanned from 30 *m/z* to 500 *m/z* at a rate of 1.5 scans/s.

3. Acids/Phenols UV analysis

a. UV absorbance calibration curve

A solution of 1000 ppm of gallic acid was created. 0.5 ml of this solution was taken, and water was added to it to create 11 different concentrations (900, 800, 700, 600, 500, 400, 300, 200, 100, 50, 25 ppm) by changing the volume of gallic acid in water. Then, 2.5 ml of folin-ciocalteu reagent 0.2 N was added to each solution which was then kept in the dark for 5 minutes. 12 mL of distillate water was added to it to get a total of 15 mL sample, and the mixture was put again in the dark for 1 hour. At the end, a spectrometer was used to measure the absorbance at 610 nm of each sample and create a calibration curve. A linear calibration curve was found as shown in Figure 1, with an equation of the form:

$$\text{Absorbance} = 9\times10^{-4}\times\text{Concentration} \tag{1}$$

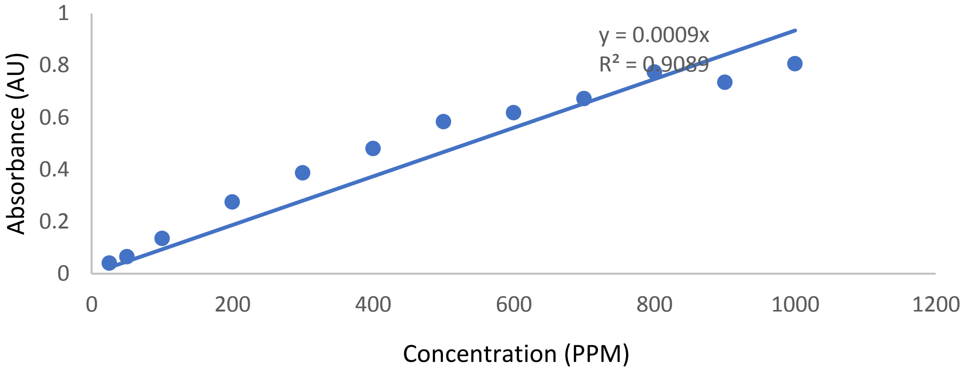

Figure 2: Acids-phenols UV absorbance calibration curve

b. <u>Liquid products UV analysis</u>

0.5 mL of each HTC experiment liquid product was taken and 2.5 mL of Folin-Ciocalteu reagent 0.2 N was added to each solution, which was then kept it in the dark for 5 minutes. 2 ml of calcium carbonate (75 g/L) was added to the mixture to neutralize it. Then, 10 mL of distillate water were added to reach a total sample volume of 15 mL, and the solution was again kept in the dark for 1 hour. Each sample was filtered using a 5 mL syringe with filter, and a spectrometer was used to measure the absorbance at 610 nm of each sample. The results are shown in Table 7 below.

Table 7: Products UV absorbance

Ratio	**Duration**	**Absorbance (AU)**
1.5	2h	2.989

1.5	4h	3.569
2.5	2h	3.411
2.5	4h	2.549
3.5	2h	2.756
3.5	4h	1.82
3.5	8h	1.64
5	2h	2.262
7	2h	1.748
9	2h	1.883
9	8h	1.146

Using calibration data, the concentration of the total acids-phenols content in gallic acid can be calculated for each sample.

CHAPTER IV

RESULTS AND DISCUSSION

A. Mass balance

Table 2 shows the reaction yield for each experiment carried out. The water-sludge ratio varied widely from 1.5 up to 9 along with a reaction time variation between 2 hours, 4 hours, and 8 hours. The temperature was kept constant at 250℃ to visualize the effect of reaction time and water-sludge ratio at the highest carbonization level possible.

As the water-sludge ratio and reaction time increased, the quantity of gas generated improved to reach a maximum of 41.9g at ratio 9 and reaction time 2 hours, and a total maximum of 50.2g at ratio 9 and reaction time 8 hours. As the residence increased, more time is allowed for the solution to go from the solid to liquid to gas phase and hence to increase the gas content. In addition, water presence promotes decarboxylation and hence increasing water content will increase CO_2 emission due to the increase in the carboxyl and carbonyl group degradation [16, 17]. That was reported in other studies where they have found that more than 85% of the gas is CO_2 [18, 20]. In addition, water plays the role of catalyst, reactant, and solvent at the same time facilitating hydrolysis, ionic condensation, and cleavage [16, 17]. Consequently, as the dilution factor increased, the process reactions intensified and reached equilibrium faster; hence promoting more degradation of the solid waste. As a result, the solid phase (hydrochar) mass decreased from 18.2g at a dilution factor 1.5 and 2 hours reaction time to 1.7g at a dilution factor 9 and 2 hours or 4 hours reaction time.

On the other hand, according to Table 1, the carbohydrates content is around 8% which is very low. Hence, the hydrochar yield was low (<36%) and decreased as the operating condition became higher. Furthermore, as the dilution factor increased, more organic materials diffused from the solid to the liquid phase leading to a decrease in the hydrochar yield.

B. Elemental analysis

As shown in Table 3, the carbon percentage remained approximately constant at different dilution factors. However, it increased slightly when reaction time increased. In all cases, the carbon content was very high (around 72-73%) in all the samples. Compared to the raw material, the carbon content increased about 1.5 times. Hence, dilution factor had no effect on carbonization and HTC was effective even at low reaction time.

On the other hand, the oxygen content decreased as the reaction time increased due to increasing the degradation level of the organic compounds. That is in accordance with the decrease in the volatile matter. However, it slightly increased when the dilution factor increased due to the increase in the water content. Compared to the raw material, with increasing reaction time and dilution factor, oxygen percentage decreased sharply from 35% to 10% which was a clear evidence of both degradation (mainly hydrolysis and decarboxylation of lignocellulose) and diffusion to the liquid phase that were happening. Nevertheless, hydrogen and nitrogen remained constant similar to previous studies [20, 23, 25].

Metals content slightly varied throughout this work. Even though each metal percentage was deficient, its variation was clear from condition to another. Magnesium and Phosphorous did not change significantly with the operating conditions. Aluminum, Potassium, and Calcium decreased as the operating conditions became high. Similarly, chlorine decreased mainly due to dichlorination and diffusion to the liquid phase [20, 23].

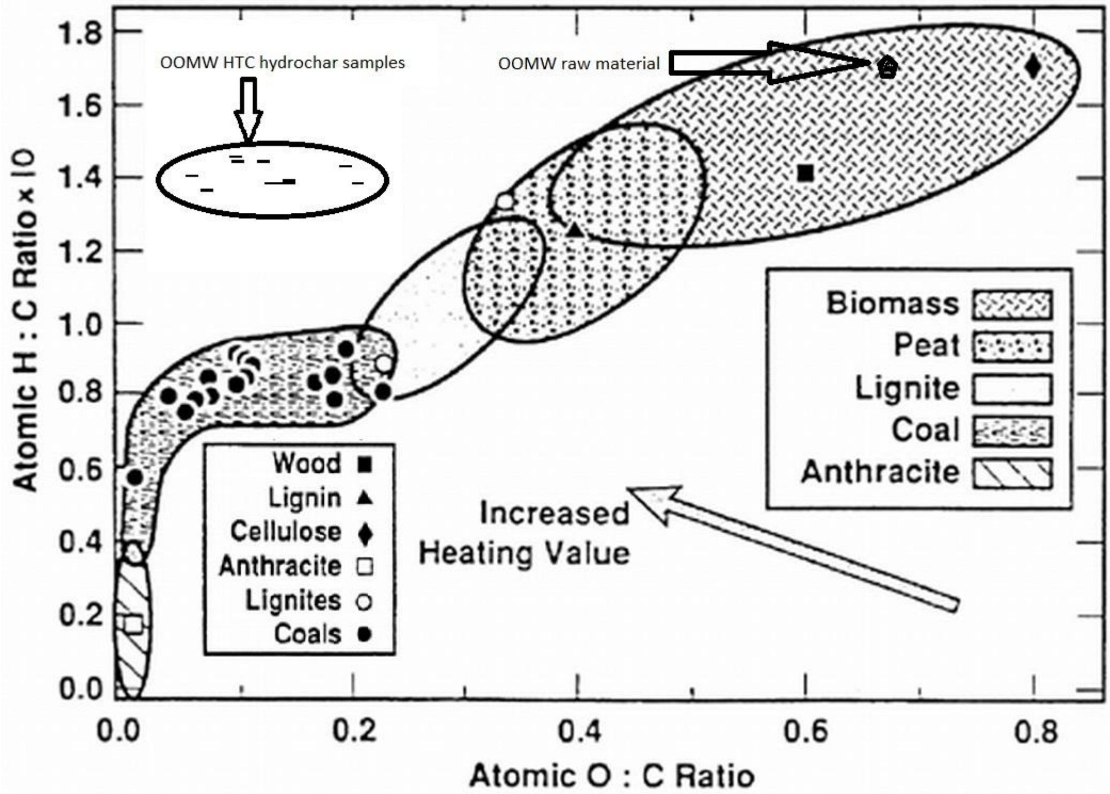

Figure 3: van-Krevelen diagram of native OMW, HTC-products, and other materials [11, 20]

From the elemental analysis results, H/C (x10) and O/C ratios were calculated in Table 4 and plotted in Figure 3. Both H/C and O/C ratios slightly increased as the dilution ratio increased due to the increase in the water content inside the reactor. However, as the reaction time increased, H/C ratio slightly decreased whereas O/C ratio reduced by a factor of 10 due to the increase in the rate of dehydration and decarboxylation reactions that were taking place. Hence, decarboxylation reaction was higher than dehydration as reported in previous work [20, 23, 25], but both lead to the production of more aromatic compounds which is in accordance with previous work [20] and with the SEM results in this work. Dehydration and decarboxylation reactions both promote degradation of the long chain heavy organic compounds into simple organic materials by the loss of a water molecule or a hydroxyl/carboxyl group (with minor production of CO2) respectively. The location of the OOMW raw material in the Van-Krevelen diagram is a clear evidence of their biomass ratio. However, the position of the unsaturated hydrochars in the same diagram shows their unique characteristics with high H/C and very low O/C ratios. Consequently, this leads to very high heating values and high carbon percentage compared to other materials (i.e. wood, coal, cellulose, etc.) along with low volatile and moisture contents. All this is in accordance with the ultimate analysis, proximate analysis, and calorific values measurements.

C. Proximate analysis

Olive oil mill waste is rich in lignocellulosic content. Hence, for lignocellulosic biomass, the cell walls are rich in hydroxyl groups and moisture can be absorbed to them [20]. With increasing reaction time and temperature, these hydroxyl group degrades, mainly by hydrolysis followed by dehydration, jointly with the hydrolysis of hemicellulose and cellulose to monosaccharides. Therefore, the moisture that can be absorbed decreased as the reaction time increased. On the other hand, as the dilution factor increased, more water is added to the system, and hence more moisture is retained in the samples.

Using contact angle measurements in Table 6, it was clear that the hydrochars are hydrophilic. This is mainly due to the retention of some phenols and lignin along with other organic materials, such as organic acids and esters, inside the hydrochars. These volatile materials are highly hydrophilic and enhance the capturing of water molecules inside the hydrochar pores.

As both reaction time and dilution factor increased, degradation level increased by hydrolysis, decarboxylation, and dehydration which in turn led to an increase in the organic material degrading and diffusing to the liquid phase. Consequently, hydrochar volatile matter decreased as the operating conditions increased. In addition, it was clear that even at the lowest operating condition (i.e. 2H - W/S = 1.5), the volatile matter in the hydrochar was much higher (i.e. 62g) than in the raw material (i.e. 19g). This sharp increase between the raw material and the hydrochar at lower operating conditions is mainly due to HTC reaction where degradation started to happen, and volatile materials began to form. This shows the effectiveness of the HTC process as a treatment technique for this waste.

The ash content decreased slowly as the reaction operating conditions became high. In fact, as the dilution factor increased, inorganic materials diffused more to the liquid phase leading to a slight decrease in the ash content. The sharp increase in the ash content at higher reaction time (i.e. 8 hours) might be just due to calculation issue since it is covering the loss resulting from the sharp decrease in the moisture and volatile matter percentages at high operating conditions. However, in most of the samples, the ash content slightly decreased compared to the raw material and stayed fixed at around 4%. The other 2% diffused to the liquid phase.

The fixed carbon or the total amount of solid carbon that remained after the reaction in the hydrochar decreased as the reaction time and dilution factor became high. This is mainly due to the increase in the degradation level with the increase in reaction time and dilution factor. In addition, more organic compounds containing carbon diffuse to the liquid phase. However, at lower reaction time and dilution factor, the total carbon percentage was higher which is in accordance with the higher hydrochar yield. A secondary char formation might have happened too since the dilution factor was low (i.e. 1.5) and the temperature was fixed at 250℃ which is high for HTC process [19].

The bulk density of the hydrochar products decreased with the increase in reaction time and dilution factor. As the dilution factor increased, the reaction became faster, and the diffusion effect became more evident along with the degradation level. In addition, with improving the reaction time, more of the solid material was degrading and diffusing to the liquid phase, leading to a decrease in the bulk density. This was in accordance with the reduction in the hydrochar yield and the fixed carbon as the reaction time and dilution factor increased.

D. XRD Analysis

The signal in Figure 4 refers to a highly amorphous structure. This is usual since the carbon content in the solid product is very high so there is no crystal structure at all [37]. Besides, according to previous researchers [38, 39], HTC destroys any crystal structure in the raw material due to the degradation of cellulose that starts at a temperature of 220℃, which is less than the operating temperature of 250℃. Figure 4 shows the behavior of a solid sample at a dilution factor of 3.5 and a reaction time of 8 hours. However, all the other samples followed the exact same trend. The small peak between 16° and 24° refer to graphite structure. Graphite is the most stable crystalline allotrope of carbon. Its characteristic peak is at 26.5°, but it was shifted to the left due to the oxygen functionalities coming from the polar groups that were retained in the hydrochars according to the FTIR results and the ultimate analysis. This is in accordance too with the amorphous layers at low operating conditions and filament structures at higher operating conditions, that were identified using SEM analysis in the following section.

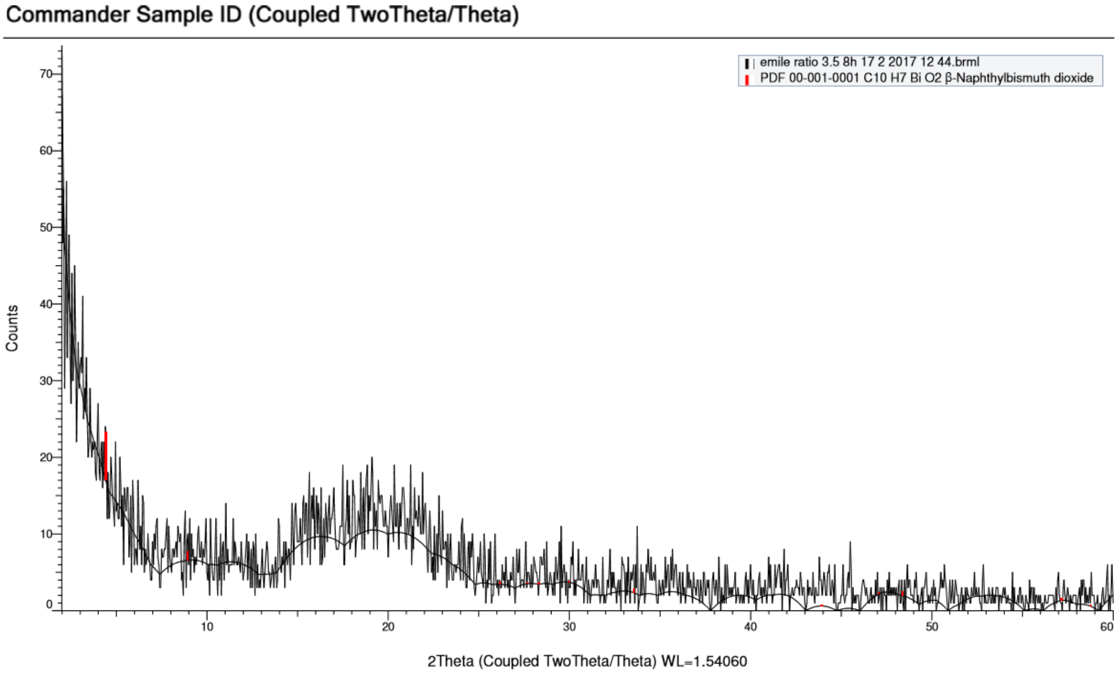

Figure 4: XRD result

E. SEM analysis

Figure 5 shows the SEM results for each experiment conditions.

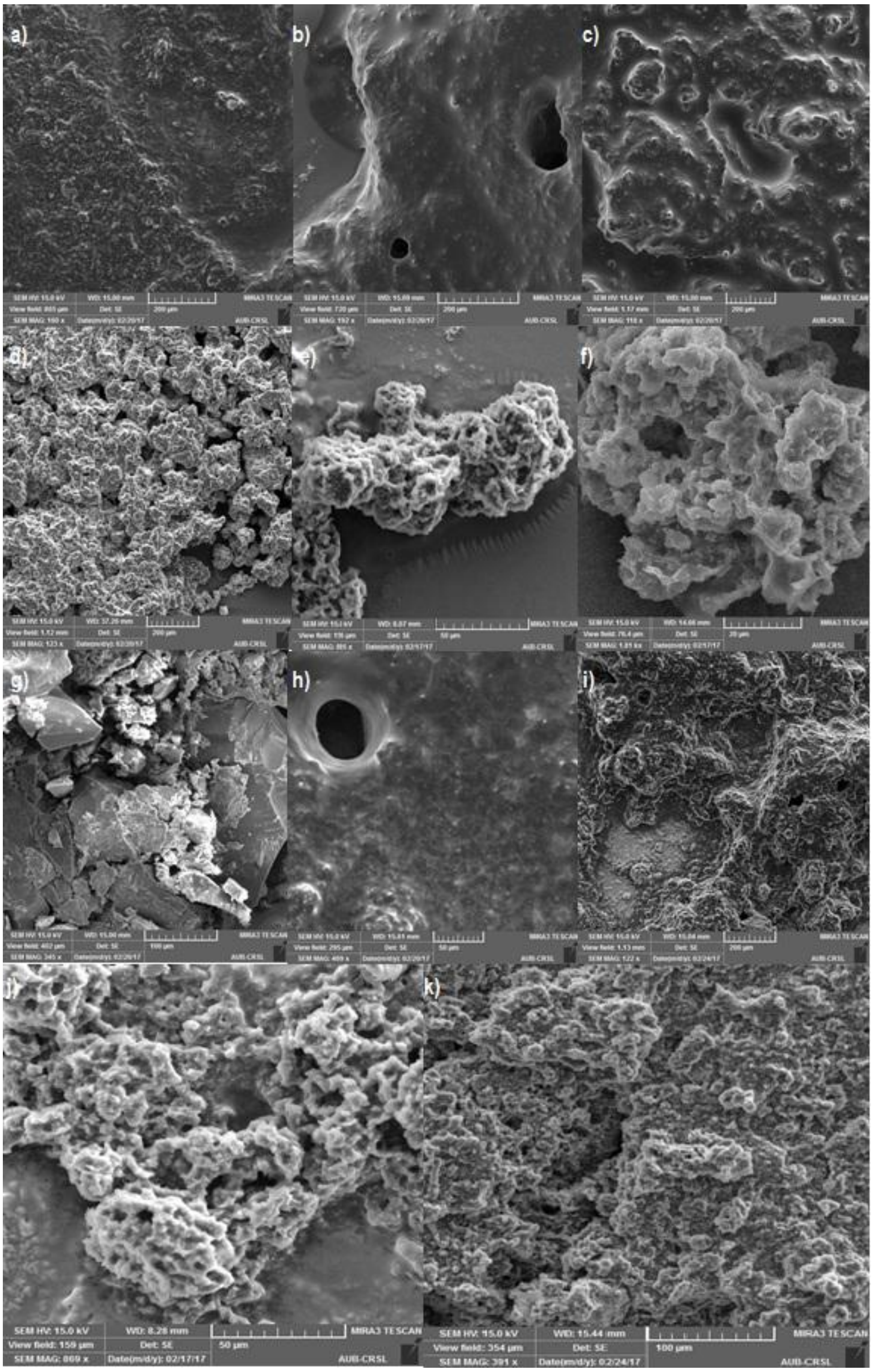

Figure 5: SEM results a) 2H - W/S = 1.5, b) 2H - W/S = 2.5, c) 2H - W/S = 3.5, d) 2H - W/S = 5, e) 2H - W/S = 7, f) 2H – W/S = 9, g) 4H – W/S = 1.5, h) 4H – W/S = 2.5, i) 4H – W/S = 3.5, j) 8H – W/S = 3.5, k) 8H – W/S = 9

All these images were taken at the microscale level. XRD results showed an amorphous structure of the hydrochar. However, despite the absence of crystal structures, it was clear from these images that as the dilution factor increased, the pore size increased, and some shapes of aromatic fiber started to appear at specific ratios. At low ratios, the amorphous structure was clear, and the pores were absent. However, as the ratio increased to 5 at 2 hours, pores and fiber shapes started to appear, and grew as the ratio kept increasing. Hence, the solid could retain a significant quantity of water, and that might explain the high moisture content at high ratios. The primary cause of this behavior was the increase in degradation and dissolution of the organic compounds as more water was added to the apparatus, specifically due to decarboxylation and aromatization reactions. As a result, the more water added to the reaction, the higher the absolute carbon loss per unit mass of feedstock to the liquid phase [17]. Hence, more microspheres and aromatic chains started to appear, and the fixed carbon decreased as it was evident in the proximate analysis. Besides, increasing water content promoted the ion mechanism pathway that took place during the reaction along with polymerization and aromatization steps.[16, 17] Thus, solids in the form of fibers and chains started to appear and to form pores.

On the other hand, as the reaction time increased, fibers started to form at a lower dilution factor. This was due mainly to the fact that the reaction was given more time, so more degradation and dissolution were happening at the same factor. From the SEM images, fibers started to appear at a dilution factor of 5 with 2 hours reaction time while the amorphous structure was still evident at a dilution factor of 3.5. However, as the reaction time increased to 4 hours and 8 hours, fibers started to appear at ratio 3.5. This is also related to the moisture content that increased as the reaction time increased and the fixed carbon that decreased with time. In addition, by allowing more time for the reaction, more organic compounds degraded or dissolved in the liquid phase which made way for the carbon fiber shape to become more explicit and hence increasing the carbon content with the increase in reaction time.

F. TGA-FTIR analyses

The TGA-FTIR results confirmed the presence of different polar groups in the hydrochar. Carboxylic acids varied from hexanoic to decanoic acids along with their derivatives. In addition, numerous ketones such as decan-one and its derivatives existed in the hydrochars. This explains the hydrophilic nature of the hydrochar since polar compounds attract water. Furthermore, Oleic acid, which is a major derivative of olive oil, existed in the hydrochars. According to Figure 6, calorific values of the hydrochar samples were slightly higher than pure carbon. This is mainly due to the presence of Oleic acid that was retained in the hydrochar. This observation explains also the oleophilic nature of the hydrochar that made the BET analysis impossible to be done without calcination.

G. BET analysis

The average BET surface area was found to be 18.16 m^2/g, and the average pore size 325 Å (32.5 nm). These values did not change significantly between the samples. The oleophilic nature of the hydrochar hindered the BET analysis. Nitrogen and Helium gases were not able to flow through the pores of the samples since they were blocked with oil. As a result, prior calcination of the samples was needed to run the BET analysis. Calcinated samples can provide a rough estimate of the surface area and pore size of the real samples.

The surface area and the pore size of the calcinated samples were both small. This explains the hydrophilic and oleophilic nature of the hydrochars since small pores retain more water and small oily surface areas retain more oil on the surface. On the other hand, it will be difficult to use the hydrochar in any adsorption processes, making it a good candidate for energy production.

H. Energy content

According to Figure 6, HTC process was not just able to treat the OOMW waste, but also to increase its energy content from 10 MJ/Kg to around 36 KJ/Kg. Compared to other materials, hydrochar calorific values were higher than that of coal, charcoal, coke, and even anthracite. The hydrochar energy values slightly changed from one sample to another, with an average value of 36 MJ/Kg. This is directly related to the high carbon content, with an average of 72%, that also remained constant in all the samples. Hence, HTC was able to increase the calorific values of the waste, even at lower reaction time and dilution factor.

Compared to pure carbon, the calorific values of the hydrochars were slightly higher, due to the oleophilic nature of the hydrochars explained by the BET and FTIR analysis results. The moisture content also varied from one sample to another, but its effect was not seen since all the samples were dried at 100℃ in an oven for 30 hours, before measuring their calorific values. However, calorific values should have decreased as moisture content increased with increasing the dilution factor and decreased with increasing the reaction time.

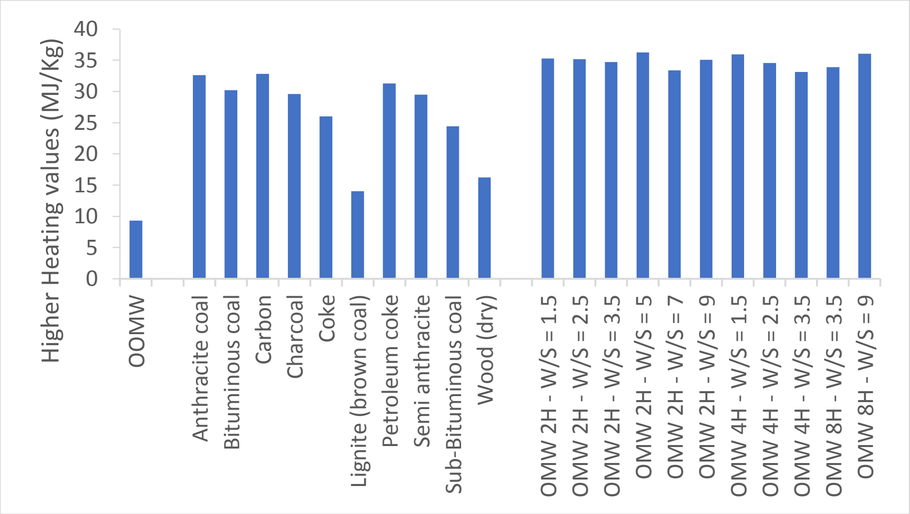

Figure 6: Higher heating values [28]

I. Liquid product analysis

All the compounds in Tables 8 and 9 were detected by GC-MS. These tables show some of the main compounds while the detailed analysis is provided in the Appendix.

Table 8: results of GC-MS acids-phenols characterization method

	Components		Components
Alcohols	(3-Methyl-oxiran-2-yl)-methanol	**Dienes**	1,2-Pentadiene
	(S)-(+)-2-Pentanol		1,4-Hexadiene, 4-methyl-
	Ethanol		1,3-Nonadiene, (E)-
Acids/esters	Propanoic acid		1-Methoxy-1,4-cyclohexadiene
	Acetic acid	**Acetates**	1-Pentadecanol acetate
	Crotonic acid		1-Tetradecyl acetate
	Pentanoic acid, 4-oxo-		6-Heptenyl acetate
	Hexanoic acid	**Glycols**	Glycerin
Ketones	Ethanone, 1-(3-pyridinyl)-		Thiodiglycol
	2-Hexanone, 6-hydroxy-	**Nitriles**	Hexadecanedinitrile
	3-Pentanone, 1,5-dimethoxy-		Undecanenitrile
	Cyclopentanone, 3-butyl-	**Amides**	2-Butenediamide, (E)-
	Cyclohexanone		Acetamide
Aldehydes	Propanal, 3-methoxy-	**Amines**	1-Propanamine, N,2-dimethyl-
	2-Hexenal, (E)-		1,2-Benzenediamine
	2-Nonenal, (E)-		1-Butanamine, N-methyl-
Phenols	Phenol		1-Pentanamine, N-methyl-
	Phenol, 2,6-dimethoxy-	**Alkanes**	(E)-2-Butenylcyclopropane
	Phenol, 2-ethoxy-		Ethane, methoxy-
	Phenol, 2-ethyl-		Heptane, 4-ethyl-
	Phenol, 2-methoxy-		Cycloheptane
	Phenol, 2-methyl-	**Alkenes**	4-Cyanocyclohexene
	Phenol, 4-ethyl-2-methoxy-		4-Decene
	Benzene ethanol, 4-hydroxy-		Cycloheptene

	Benzyl Alcohol	Flavones	2(1H)-Pyridinone
	Benzyl alcohol, 4-fluoro-3-methoxy-		Butyrolactone
	Homo-vanillyl alcohol		Hydroquinone
	Phenyl-ethyl Alcohol		4-Pyridinol
Diones	1,3-Cyclohexanedione, 5,5-dimethyl-	**Flavonols**	D-Arabinitol
	3,6-Diisopropylpiperazin-2,5-dione		dl-Threitol
Diols	2-Ethyl-2-methyl-1,3-propanediol		
	1,2-Benzenediol		

Table 9: results of GC-MS polyaromatic hydrocarbon characterization method

	Components		**Components**
Alcohols	1-Pentanol, 2,3-dimethyl-	**Alkanes**	Butane, 2-methyl-
	2-Hexanol		Hexane
	Cyclohexanol		Heptane
	Cyclopentanol, 1-methyl-		Octane
	Benzeneethanol, 4-hydroxy-		Nonane
Acids / esters	Nonahexacontanoic acid		Decane
	Cyanic acid, propyl ester		Tetracosane
	Oxalic acid, allyl decyl ester		Tetratetracontane
	Nonanedioic acid, dihexyl ester		Tetratriacontane
	Sulfurous acid, butyl dodecyl ester		Triacontane
Ethers	1,2,3-Propatriol, 1-indol-4-yl(ether)		Tridecane
	Methyl octyl ether		Undecane
Ketones	Ethanone	**Alkenes**	1-Propene, 2-methyl-
	Propanone		1-Pentene, 2,3-dimethyl-
	Cyclohexanone, 2-butyl-		1-Hexene
	2-Heptanone, 4-methyl-		1-Heptene
	2-Nonanone		1-Nonene
Diones	2,3-Furandione, dihydro-4,4-dimethyl-		1-Docosene
	2,4-Hexanedione		2-Undecene, (Z)-
	3,3-Dimethyl-2,4-pentane dione		Toluene
	3,5-Heptanedione, 2,2,4,6-tetramethyl-	**Alkynes**	1-Nonyne
Aldehyde	2-Hexenal, (E)-		2-Hexyne

s	Benzaldehyde Hexanal Octadecanal Nonanal
Phenols	3,4-Dimethylbenzyl alcohol Phenol Phenol, 2,4-bis(1,1-dimethylethyl)- Phenol, 2,4-bis(1-phenylethyl)- Phenol, 2-methoxy- Phenol, 2-propyl- Phenol, 4-ethyl- Phenylethyl Alcohol

Dienes	1,15-Hexadecadiene 1,4-Pentadiene 1,6-Heptadiene
Amines	1,3-Propanediamine, N-methyl- 2-Butanamine, (S)- 2-Pentanamine n-Hexylmethylamine
Flavones	2(3H)-Furanone, dihydro-3-methyl- Di-n-decylsulfone Butyrolactone
Flavonols	1-Hexacosanol 1H-Imidazole, 1-methyl-4-nitro-

It is obvious in Figure 7 that as the water-sludge ratio and reaction time increased, the height of all peaks decreased indicating a lower acids-phenols concentration. In addition, most of the compounds in both Figures 7 and 8 eluted at the same retention time indicating that the compositions of the samples are not different from one to another.

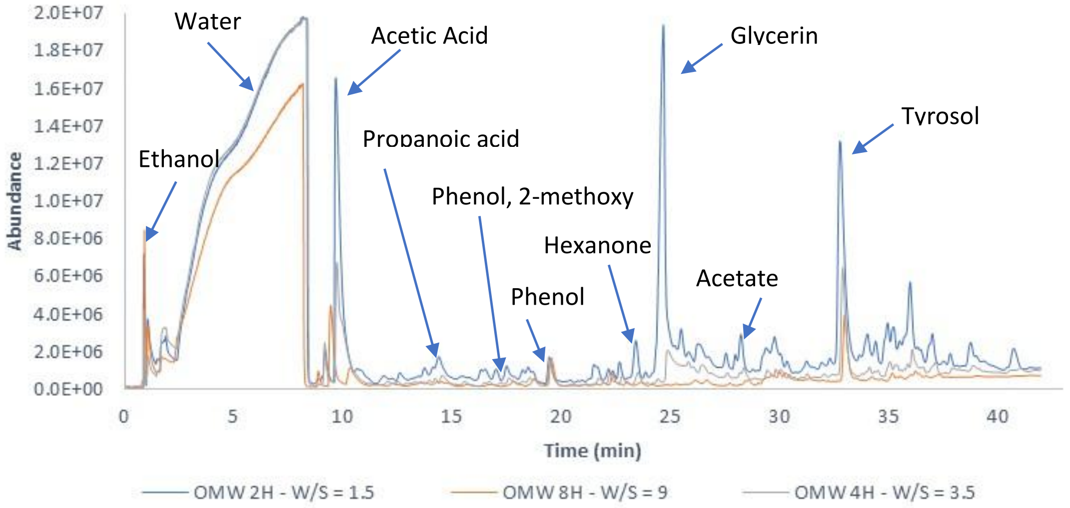

Figure 7: chromatogram of acids-phenols characterization method

Similarly, from the peaks in Figure 8, it can be concluded that the hydrocarbons concentration decreased as the water-sludge ratio and reaction time increased (e.g.

ratio/duration of 1.5/2h, 9/8h, 3.5/4h). This shows clearly the effect of changing these operating conditions on the liquid phase product. A detailed identification for all the peaks for each sample is presented in Appendices A and B.

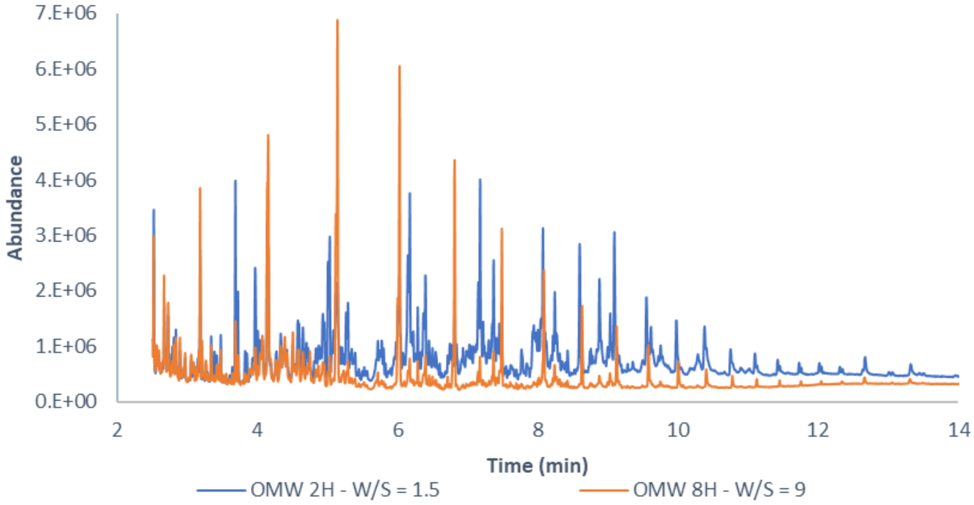

Figure 8: chromatogram of polyaromatic hydrocarbon characterization method

The method used in figure 8 focused on polyaromatic hydrocarbons detection. However, their concentration seemed to be negligible since the operating temperature was at 250°C which is much lower than their formation temperature (of 300°C). This is in accordance with other findings [25, 40]. Hence, the method developed in section 2.4 is ideal for hydrocarbons and organic acids detection.

Previous works confirmed that the olive oil mill wastewater contains a small quantity of organic material (around 10%), proteins (around 7.5%) and carbohydrates (around 8%). However, the lignin content was very high (around 20%) along with simple biophenols [1, 10, 11, 25]. The proteins proteolyzed and broke down into smaller proteins which remained mostly in the hydrochars while most of the amino acids were transferred to the liquid phase and hydrolyzed further into amine and amide derivatives. That was clear from the presence of 1-propanamine, N,2-dimethyl-, 2-butanamine, 3-methyl-, and other short chain amine derivatives at lower water to sludge ratio, to 1,2-benzenediamine, 1-pentanamine, N-methyl- and other longer chain amine derivatives at high water to sludge ratio. Further proteolysis leaded to the production of some phenolic substances along with ammonia which was present in all the samples with a very good concentration. This leads too, to the production of low molecular weight organic acids including lactic acid, propanoic acid, and acetic acid. It should be noted that 2-pyrrolidinone existed in all the samples. That is primarily due to the interaction between ketones and ammonia or hydrogenation of amines.

Carbohydrates and sugars undergo decomposition by hydrolysis to give alcohols and organic acids, or other oxygenated species, such as ketones, aldehydes, esters, and ethers [16, 25, 26, 41]. That was evident, in Figure 7, from the presence of a large peak for pure ethanol at an elution time of 2 minutes with another peak at an elution time of around 10 minutes for acetic acid. These two compounds were produced in an anaerobic environment in all the samples. Secoiridodes in the oily raw material degraded by hydrolysis to oleuropein aglycons that degraded further to aldehydes. The oleuropein aglycon is absent in all the samples since its degradation starts at a temperature lower than 230°C while the operating temperature was always fixed at 250°C. However, most of the aldehydes in all samples existed at milder operating conditions and were totally absent at the extreme cases. This is mainly due to fact that as the reaction time increased, more degradation was taking place; and with increasing the water contents, degradation was accelerated, and the aldehydes underwent decarboxylation to produce alkanes.

The presence of glycerol in all samples along with some fatty acids such as butanoic acid, pentanoic acid and their derivatives along with 2,3-diazatetracyclo [3.3.0.0(4,7).0(6,8)] octane-3-carboxylic acid and other long chain acids, gives a clear evidence of lipid degradation. Hemicellulose and cellulose content were very low in the raw material. However, their degradation can affect the final products. Hemicellulose hydrolyze to sugar monomers at around 180°C and cellulose to oligomers at 230°C. The sugar monomers decompose to Dione derivatives that contains two ketone groups, then to acids and ketones by decarboxylation. All the diones such as 2,5-piperazinedione, 3-methyl-6-(1-methylethyl)-, 3,6-diisopropylpiperazin-2,5-dione, and others were just detected at a water to sludge ratio of less than 3.5. Hence, the degradation was not complete yet under these conditions. On the other hand, less reactive oligomers hydrolyzed further to glucose and then to acids and alcohols. Glucose was absent in all the samples which means that the operating temperature (of 250°C) was enough to degrade it all. Highly reactive oligomers polymerized and aromatized to produce some cycloketones and cycloacids such as 6-hydroxy-9-methyl-9-aza-bicyclo [3.3.1] nonan-3-one and 6-hydroxymethyl-5-methyl-bicyclo[3.1.0]hexan-2-one, bicyclo [2.2.2]octane-1-carboxylic acid, and others.

The minor existence of esters and ethers in all the samples was primarily due to hydrolysis of the ester bond followed by decarboxylation and dehydration reactions to produce ketones and carboxylic acids. This hydrolysis is a direct function of temperature. Hence, since the operating temperature in all the samples was one of the highest for hydrothermal degradation (250°C), hydrolysis of the ester bond was happening early in the apparatus with minor concentrations remaining at the end.

On the other hand, heavy molecular weight ketones were produced from hydrolysis of the raw material (lignin, cellulose, hemicellulose, carbohydrates, etc.) along with dione derivatives, such as 3,11-diazabicyclo [4.4.1]undecan-4-one, 11-methyl-, and cyclohexanone. These existed especially at shorter reaction times and lower ratios as illustrated in the appendix. However, as the reaction time and ratio increased, further degradation happened and the loss of the carbonyl group by decarboxylation promoted the formation of smaller molecular weight ketones such as 3-pentanone, 1,5-dimethoxy-, and carboxylic acids such as propanoic acid, butanoic acid, propanoic acid, and others. Amide derivatives existed too at lower ratios and shorter reaction times. They are carboxylic acids derivatives, and produce esters and ethers from fats, lipids, and mostly lignin hydrolysis. They might condense and hydrolyze further to produce different types of alcohols, ketones, fatty acids, aliphatic acids, and even aldehydes. However, these amides can follow another path to convert to nitriles by dehydration. Some of the long chain nitriles existed at milder operating conditions such as hexadecanedinitrile and undecanenitrile, or shorter chain at harsh operating conditions such as butanenitrile, 4-(methylthio)-. This difference is primarily due to aromatization and polymerization as the reaction time and water content increase.

Dehydration of alcohols also promote the formation of long chain alkenes such as decene, and diene derivatives. Most of the alkenes were formed at lower ratios and shorter reaction times. Nevertheless, at longer reaction times and higher ratios, these long chain alkenes transform to alkanes by aromatization and polymerization. On the other hand, dehydration of alcohols promotes ethers and esters formation. However, if it is followed by decarboxylation, the loss of the carboxyl group produces alkanes. From the table in the appendix, as the reaction time and ratio increased, more degradation happened and shorter chain alkanes such as ethane, propane, and their derivatives were formed instead of the longer ones at shorter reaction time and lower ratio.

Lignin exists at high concentrations in the raw material [1, 10, 11, 25]. It consists of various polyphenolic compounds that are linked mainly by ether bonds.

Hence, under hydrothermal carbonization, the α-O-4 and β-O-4, that connect the lignin molecule, dissociate by hydrolysis [41] due to their low bond dissociation energy. However, more than 60% of the lignin bonds are β-O-4 while less than 7% are α-O-4[42, 43]. Other types of bonds exist too but in minor percentages[42, 43]. On the other hand, the measured pH of the raw material had a value of 2, hence, cleavage of β-O-4 bonds, under acidic conditions, governs the lignin degradation mechanism.

As illustrated in Figure 9, during cleavage reaction, β-O-4 bond at the β position (I) converts primarily into benzyl cation intermediate (II) by protonation, and an enol ether type of structure III is formed (route A). In the presence of water, further hydrolysis and cleavage of the ether bonds and β-O-4 bond happen to produce simple phenols (IV) and Hibbert's ketone (V). Route B compete with route A where formaldehyde is released from II and another enol ether forms (VI) [36, 42]. The β-O-4 bond of VI is similarly hydrolyzed to yield the phenol IV along with an aldehyde VII [42]. Guaiacol decomposes to produce benzenediols, but the benzene ring is stable under hydrothermal conditions and the energy of the aliphatic C-O bond is lower than the aromatic's [24, 25, 41]. Hence, the conversion of these aromatic products might be primarily due to the hydrolysis of the aliphatic C-O bond of the methoxyl group leading to the formation of carboxylic acids and alcohols (see table in the appendix), especially acetic acid that is a major product in all the samples with a high GC-MS peak. Benzeneethanol, 4-hydroxy- or tyrosol, phenol, phenol, 2-methoxy-, homovanillyl alcohol, and phenylethyl alcohol, that existed in all samples are clear evidence of lignin degradation. The existence of other phenol derivatives was dependent on the operating conditions and increased as it became more severe. Further dehydration and polymerization of these molecules produced some alkenes or even alkanes at the HTC high temperature of 250°C.

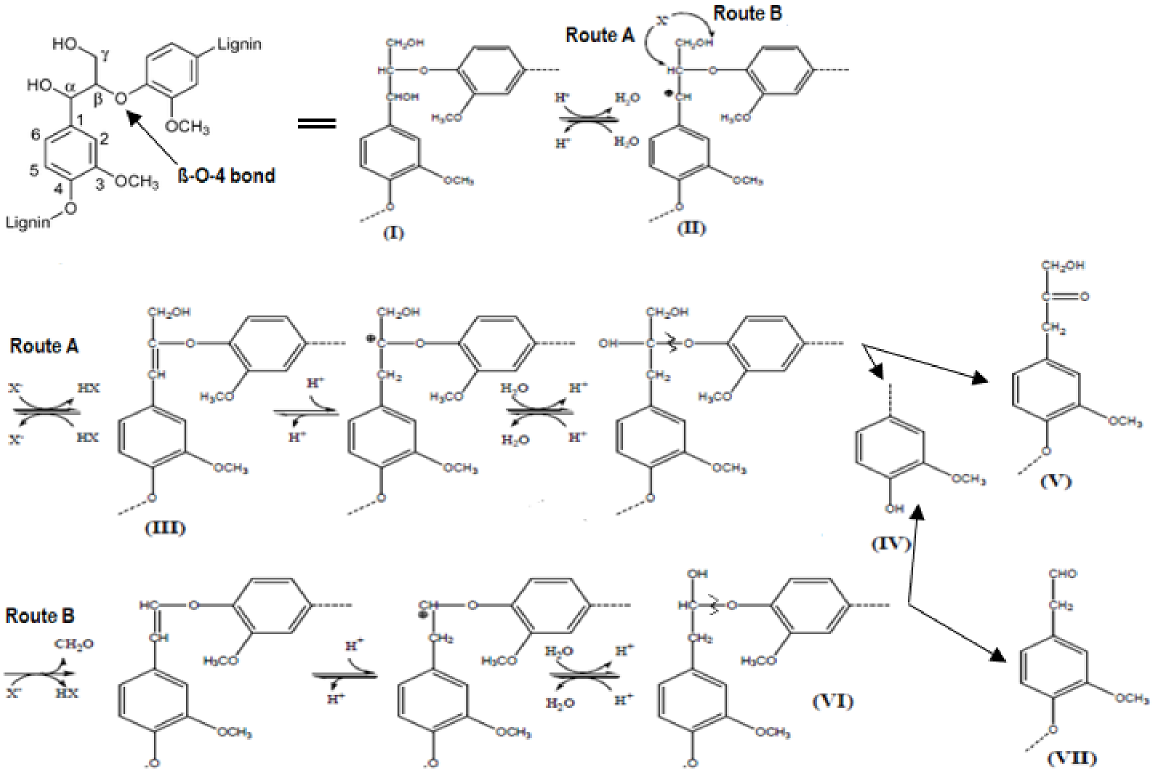

Figure 9: mechanism of the β-O-4 bond cleavage based on Lundquist and Lundgren's research

It should be noted that numerous flavones and flavonols were detected in all experiments. They originate from the oily raw material rich in antioxidants in small concentrations. Most of these existed at milder operating conditions such as 2(1H)-pyridinone, 3,11 diazabicyclo[4.4.1]undecan-4-one, 11-methyl- and dl-threitol. However, with increasing reaction time and ratio, these complex flavones and flavonols degrade into simpler components such as thiazole, 2-butyl-4-methyl-, trans-1,10-dimethyl-trans-9-decalol, 5,6,7,8-tetrahydro-thiazolo[5,4-c] azepin-4-one, along with other biophenolic acids such as benzoic acid, crotonic acid, and others.

As mentioned earlier, two main methods were used in this work for the liquid phase analysis: method 1 focused on the acid-phenols analysis, and method 2 focused on the non-polar compounds analysis (such as polyaromatic hydrocarbon). In method 1, water was used for solvent extraction which acted at the same time as solvent and catalyst for the reaction. In method 2, a mixture of acetone-hexane was used for solvent extraction. Water is extremely polar, even much more polar than acetone while hexane is non-polar. Hence, despite detecting many compounds using the two methods, differences between the two existed is due to several factors, including:

- Difference between the corresponding GC-MS methods in terms of detection limit, resolution, elution time, and temperature ramping, leading to detection of different compounds.
- Method 1 extracted highly polar compounds such as alcohols, phenols, and acids better than the second one. The latter uses hexane which is highly non-polar along with acetone which polarity is not high. Hence, method 2 extracted better the non-polar compounds (such as hydrocarbons and polyaromatic hydrocarbons), along with the slightly polar compounds such as aldehydes.
- Short chain alcohols were detected in method 1 vs long chain alcohols in method 2.
- More carboxylic acids were detected in method 1 vs more organic acids detected in method 2.
- Most of the detected ketones, diones derivatives, flavones, and flavonols were the same.
- Detection of some ethers and numerous aldehydes in method 2 while no ethers and few aldehydes were detected in method 1.
- Method 1 was better for acetate, nitrile, amides, and especially amines detection than method 2.

- Minor hydrocarbons were detected in method 1. However, using method 2, alkanes ranging from Butane to tetra-tria-contane along with their derivative, alkenes, and minor alkynes were all detected.

J. Acids-phenols quantification in the liquid product

From the calibration curve eq. (1), the total phenols concentration of each sample expressed as gallic acid equivalent can be derived in the graph below.

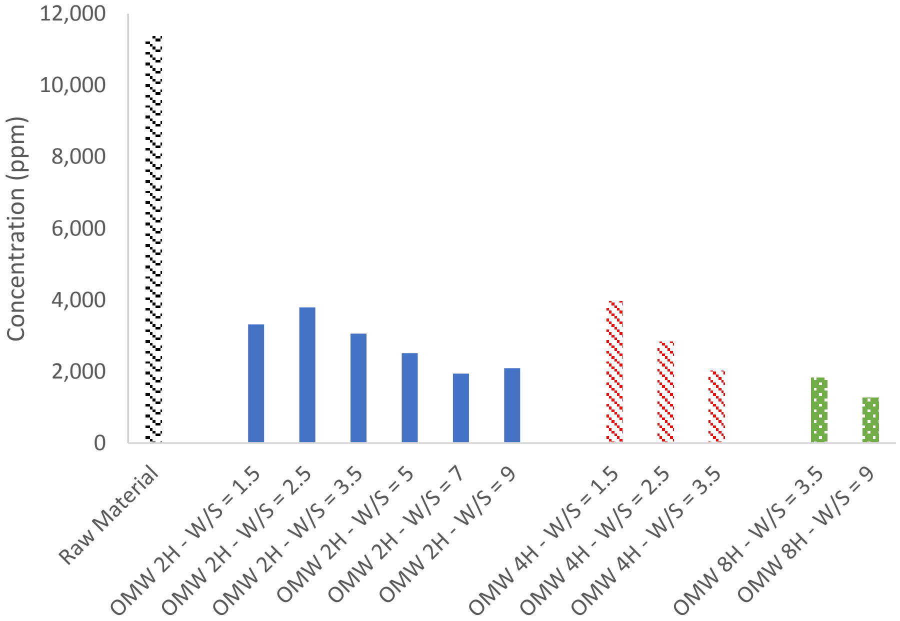

Figure 10: Total acids-phenols concentration in gallic acid in each sample

Previous researchers reported that the lignin content in the olive oil mill water is very high (~ 20% wt) along with simple biophenols [1, 10, 11, 25]. In addition, it was reported that the total phenolic content in the olive oil mill waste water depends on the season, location, land specifications, height, among other factors. It is estimated on average to be around 10,000 ppm [14, 24, 26, 44, 45]. In this work the measured total acids-phenols content of the used olive oil mill waste water raw material was 11,362 ppm.

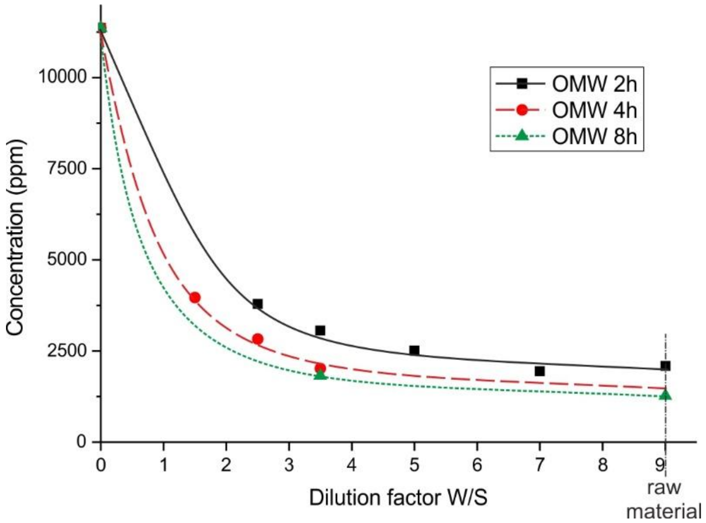

Figure 11: Acid-phenol concentrations in gallic acid with respect to dilution factors

It was obvious that as the reaction time increased, more degradation was taking place and hence most of the complex phenols and long chain fatty acids were degrading into simple phenols and simple carboxylic acids. However, the degradation of simple phenols was not achievable [26, 41], hence, the total acid-phenol concentration will hit a bottom limit. As a result, as illustrated in Figure 10, the acid-phenol concentration decreased with increasing reaction time to reach a very low level where most of the remaining acid-phenols were simple biophenols. In addition, as the dilution factor increased, more degradation was taking place, especially through hydrolysis, since water acted as a solvent and catalyst for the reaction. At the same time, increasing the water content was diluting the final product solution. As a result, simple biophenols were reached faster and at lower concentrations.

From Figure 11, the total acids-phenols exhibited a sharp decrease from 11,382 ppm to less than 3,500 ppm and continued to decrease until a dilution factor of 3.5 and followed a horizontal/asymptotic behavior afterwards. This behavior was shown for different reaction times of 2 hours, 4 hours, and 8 hours. The asymptotic reduction in concentration is due to the fact that degradation has decreased in favor of dilution.

Hence, it is anticipated that both degradation and dilution are affecting the final acid-phenol quantity.

It was obvious that the effect of degradation influenced the total acids-phenols concentration more than dilution. The difference in the compounds found in Appendix A between the samples validates this explanation. Complex phenols and long chain acids at lower dilution ratios were abundant while simple phenols and small chain acids increased with the dilution factor up to a 3.5 ratio. After the dilution factor of 3.5, the compounds found did not change much. As a result, according to figure 11 and the results in appendix A, the HTC optimum operating conditions were at a dilution factor of 3.5 and a residence time of 4 h.

Furthermore, as illustrated in Figure 10, HTC can achieve major reduction in acid-phenols concentrations from 11362 ppm to as low as 1318 ppm, under long reaction times (8 hours) and at a high water to sludge ratio of 9 that corresponds to the water fraction in the original raw material. Hence, HTC can be used to treat the raw material as is, without any prior evaporation if necessary. However, this will be accomplished at the expense of a larger reactor volume and higher energy consumption.

CHAPTER V

CONCLUSION

Olive oil mill wastewater is one of the worst marine pollutants. Its disposal in the environment without treatment has several destructive effects. Hydrothermal carbonization seemed to be a very effective treatment technique for this waste since it transformed the waste into profitable bioenergy feedstock similar to brown coal, called hydrochars. The effects of dilution factor and reaction time on the produced hydrochars were studied in detail in this work and seemed to be highly significant. Hydrochar yield was the highest at the lowest dilution factor (i.e. 1.5) and reaction time (2 hours), while carbon percentage and calorific values were significantly high and not affected by the change in the operating conditions. In addition, amorphous structure and low hydrochar moisture content were obtained at the lowest dilution factor. Consequently, hydrochar quality increased with the decrease in the dilution factor. Hence, it is better to evaporate water from the raw materials prior to HTC and operate the process at the lowest dilution factor possible, moderate reaction time, and highest temperature to obtain hydrochars with the best characteristics.

On the other hand, GC-MS and various detailed extraction and analysis methods showed that the treated liquid is rich in phenols, acids, and numerous hydrocarbons which constitute high value products. It was found that phenols and hydrocarbons concentration decreased as the water-sludge ratio (dilution factor) and reaction time increased. On the other hand, the UV analysis proved that there exists a trade-off between adopting optimum HTC conditions or treating the waste as it is without any prior evaporation. The optimum operating condition of dilution factor of 3.5 and reaction time of 4h involves evaporating part of the water phase prior to HTC treatment. This has the advantage of reduced time required for complete degradation and smaller volumes in expenses of higher energy consumption for evaporation. On the other hand, at a dilution factor of nine (same as the raw materials) and a residence time of 8h, HTC decreased the total acids-phenols content by more than 10 folds. Hence, HTC can be applied to OOMW without any prior evaporation. This requires less process steps/equipment and less energy consumption but will incur higher capital costs due to larger volume. Consequently, this should be compared against evaporation costs.

REFERENCES

1. Hashwa, F.M., Elias. *AEROBIC AND ANAEROBIC BIOTREATMENT OF OLIVE OIL MILL WASTE WATER*. February 2010 [cited 2017.
2. Feria, A.L., *The generated situation by the OMW in Andalusia.* Actas proceeding- Workshop Improlive Anexo, 2000. **A1 Annex A1 Spain**: p. 55-63.
3. Al-Khudary, R., Hashwa, F., & Mroueh, M., *A novel olive oil degrading thermoactinomyces species with a high extremely thermostable activity.* Engineering in Life Sciences,, 2004. **1**: p. 78-82.
4. Saez, L., Perez, J., & Martinez, J. , *Low molecular weight phenolic attenuation during simulated treatment of wastewaters from olive oil mills in evaporation ponds.* Water Research, 1992. **26**: p. 1261-1266.
5. Paredes, M.J., Monteoliva-sanchez, M., Moreno, E., Perez, J., Ramos-Cormenzanz, A., & Marinez, J. , *Effect of waste waters from olive oil extraction plants on the bacterial population of soil.* 1986.
6. Tuncel, G., & Nergiz, C. , *Antimicrobial effect of some olive phenols in a laboratory medium.* Letters in Applied Microbiology, 1993. **17**(300-302).
7. Pérez, J., De La Rubia, T., Moreno, J., & Martínez, J. , *Phenolic content and antibacterial activity of olive oil waste waters.* Environmental Toxicology and Chemistry, 1992. **11**: p. 489-495.
8. Ragazzi, E., & Veronese, G., *The effect of oxidative coloration on the methanogenic toxicity and anaerobic biodegradability of phenols.* Biological Water, 1989. **32**: p. 210-225.
9. Ubay, G.O., L. , *Anaerobic treatment of olive mill effluents. Water Science Technology.* 35, 1997: p. 287-294.
10. Skerratt, G., & Ammar, E., *The application of reedbed treatment technology to the treatment of effluents from olive oil mills.* Final report, ENISLARSEN - Staffordshire University, UK., 1999.
11. Lopez, R., *Land treatment of liquid wastes from the olive oil industry (Alpechin).* Fresenius Enviromental Bulletin, 1992. **1**: p. 129-134.
12. Squadrillion, L. *New Solutions for Managing Olive Mill Waste Water*. Filed in Making Olive Oil November 12, 2014.
13. Sturzenberger, N., *Olive Processing Waste Management: Summary.* UC Davis Olive Oil, University of California, Davis, 2007.
14. Antonio Fiorentino, A.G., Marina Isidori, Margherita Lavorgna, Alfredo Parrella, and Fabio Temussi, *Olive Oil Mill Wastewater Treatment Using a Chemical and Biological Approach.* journal of Agriculture and Food Chemistry, 2004. **52**(16): p. 5151–5154.
15. Giuseppe Di Lecce, A.C., Alessandra Bendini, Carmela Conidi, Lidietta Giorno, Tullia Gallina Toschi, *Characterization of olive mill wastewater fractions treatment by integrated membrane process.* Journal of the Science of Food and Agriculture, 9 April 2014.
16. Funke, A. and F. Ziegler, *Hydrothermal carbonization of biomass: A summary and discussion of chemical mechanisms for process engineering.* Biofuels, Bioproducts and Biorefining, 2010. **4**(2): p. 160-177.
17. Libra, J.A., et al., *Hydrothermal carbonization of biomass residuals: a comparative review of the chemistry, processes and applications of wet and dry pyrolysis.* Biofuels, 2014. **2**(1): p. 71-106.

18. Borrero-Lopez, A.M., et al., *High added-value products from the hydrothermal carbonisation of olive stones.* Environ Sci Pollut Res Int, 2017. **24**(11): p. 9859-9869.
19. Volpe, M. and L. Fiori, *From olive waste to solid biofuel through hydrothermal carbonisation: The role of temperature and solid load on secondary char formation and hydrochar energy properties.* Journal of Analytical and Applied Pyrolysis, 2017. **124**: p. 63-72.
20. Benavente, V., E. Calabuig, and A. Fullana, *Upgrading of moist agro-industrial wastes by hydrothermal carbonization.* Journal of Analytical and Applied Pyrolysis, 2015. **113**: p. 89-98.
21. Young-Min Kim, J.J., Soyoung Myung, Bong Hyun Sung, Jong-In Dong, Young-Kwon Park, *Investigation into the lignin decomposition mechanism by analysis of the pyrolysis product of Pinus radiata.* Biresource Technology, 2016. **219**: p. 371–377.
22. Reza, M.T., et al., *Hydrothermal carbonization: Fate of inorganics.* Biomass and Bioenergy, 2013. **49**: p. 86-94.
23. Ghanim, B.M., et al., *Hydrothermal carbonisation of poultry litter: Effects of treatment temperature and residence time on yields and chemical properties of hydrochars.* Bioresour Technol, 2016. **216**: p. 373-80.
24. El-Abbassi, A., H. Kiai, and A. Hafidi, *Phenolic profile and antioxidant activities of olive mill wastewater.* Food Chem, 2012. **132**(1): p. 406-12.
25. Poerschmann, J., et al., *Hydrothermal carbonization of olive mill wastewater.* Bioresour Technol, 2013. **133**: p. 581-8.
26. Poerschmann, J., B. Weiner, and I. Baskyr, *Organic compounds in olive mill wastewater and in solutions resulting from hydrothermal carbonization of the wastewater.* Chemosphere, 2013. **92**(11): p. 1472-82.
27. Tsagaraki, E., Lazarides, H. N., & Petrotos, K. B., *Utilisation of by-products and treatment of waste in the food industry.* Olive mill wastewater. In V. Oreopoulou & W. Russ (Eds.), Springer., 2007: p. 133–157.
28. Feki, I., Allouche, N., & Sayadi, S., *The use of polyphenolic extract, purified hydroxytyrosol and 3, 4- dihydroxyphenyl acetic acid from olive mill wastewater for the stabilization of refined oils: a potential alternative to synthetic antioxidants.* Food Chemistry, 2005. **93**: p. 197–204.
29. E. Węgrzyn, S.G., W. Popławska, and B. K. Głód, *MODIFIED ANALYTICAL METHOD FOR POLYCYCLIC AROMATIC HYDROCARBONS, USING SEC FOR SAMPLE PREPARATION AND RP-HPLC WITH FLUORESCENCE DETECTION. APPLICATION TO DIFFERENT FOOD SAMPLES.* Meat and Fat Research Institute, ul. Jubilerska 4, 04-190 Warszawa, Poland.
30. Takeo Sakuma, D.L., Carmai Seto, André Schreiber, and Rebecca Wittrig, AB SCIEX Concord, Ontario (Canada); AB SCIEX Warrington (UK); Restek Corporation, Bellefonte, Pennsylvania (USA), *Analysis of Polycyclic Aromatic Hydrocarbons (PAH), Alkylated Derivatives, and Photo-degradation Products in Environmental and Food Samples using LC-FLD-MS/MS with Q TRAP® Technology.* Food and Environmental
31. Christine Dumas, T.F., Katherine K. Stenerson, Olga Shimelis, Ken Espenschied, Michael Halpenny, Lisa Fitzpatrick, Klaus Buckendahl, and Frank Michel, *Analysis of PAHs in Olive Oil Using a New Dual-Layer SPE Cartridge for Simultaneous Extraction and Cleanup.* Sigma-Aldrich, St Quentin Fallavier

France, Supelco, Div. of Sigma-Aldrich, Bellefonte, PA 16823 USA, Sigma-Aldrich Ltd. Poole, Dorset BH12 QH, UK, 4Sigma-Aldrich Chemie GmbH, 82024Taufkirchen, Germany.

32. Christine Dumas, T.F., Katherine K. Stenerson, Olga Shimelis, Ken Espenschied, Michael Halpenny, Lisa Fitzpatrick, Klaus Buckendahl, and Frank Michel, *Analysis of PAHs in Olive Oil Using a New Dual-Layer SPE Cartridge for Simultaneous Extraction and Cleanup.* 2015.
33. *ORGANIC COMPOUNDS IN WATER BY MICROEXTRACTION, method epa-3511, November 2002.*
34. Jurek, A., *Automated Liquid-Liquid Extraction of PAH Compounds in Water.* Environmental.
35. Wu, S. and W. Yu, *Liquid–liquid extraction of polycyclic aromatic hydrocarbons in four different edible oils from China.* Food Chemistry, 2012. **134**(1): p. 597-601.
36. Haleyur, N., et al., *Comparison of rapid solvent extraction systems for the GC-MS/MS characterization of polycyclic aromatic hydrocarbons in aged, contaminated soil.* MethodsX, 2016. **3**: p. 364-70.
37. Chu, P.K. and L. Li, *Characterization of amorphous and nanocrystalline carbon films.* Materials Chemistry and Physics, 2006. **96**(2-3): p. 253-277.
38. Kang, S., Li, X., Fan, J., and Chang, J., *Characterization of hydrochars produced by hydrothermal carbonization of lignin, cellulose, D-xylose, and wood meal.* Ind. Eng. Chem. Res., 2012. **51**(26): p. 9023-9031.
39. Baobin Wang, Q.W., Guihua Yang, *Effect of Residence Time on Hydrothermal Carbonization of Corn Cob Residual.* Bioresources, 2015. **10**(3): p. 3979-3986.
40. Tymchyshyn, M., Xu, C., 2010. , *Liquefaction of bio-mass in hot-compressed water for the production of phenolic compounds.* Bioresource. **Technol.**(101): p. 2483–2490.
41. Kang, S., et al., *Classified Separation of Lignin Hydrothermal Liquefied Products.* Industrial & Engineering Chemistry Research, 2011. **50**(19): p. 11288-11296.
42. Ricardo B. Santos, P.W.H., Hasan Jameel, and Hou-min Chang, *Wood Based Lignin Reactions Important to the Biorefinery and Pulp and Paper Industries.* Bioresources, 2013. **8**(1): p. 1456-1477.
43. Patil, R.A., *Cleavage of acetyl groups for acetic acid production in Kraft pulp mills.* Thesis. University of Maine, 2012.
44. Leouifoudi, I., H. Harnafi, and A. Zyad, *Olive Mill Waste Extracts: Polyphenols Content, Antioxidant, and Antimicrobial Activities.* Adv Pharmacol Sci, 2015. **2015**: p. 714138.
45. Leouifoudi, I., et al., *Identification and characterisation of phenolic compounds extracted from Moroccan olive mill wastewater.* Food Science and Technology (Campinas), 2014. **34**(2): p. 249-257.

APPENDIX A

Table 10: Appendix A

		Ratios										
	Samples	**1.5 2h**	**1.5 4h**	**2.5 2h**	**2.5 4h**	**3.5 2h**	**3.5 4h**	**3.5 8h**	**5 2 h**	**7 2 h**	**9 2 h**	**9 8 h**
Alcohol	(3-Methyl-oxiran-2-yl)-methanol						🟦					
	(S)-(+)-2-Pentanol	🟩										
	1,4-Anhydro-d-galactitol		🟦									
	1-[N-Methylpiperazine]ethanol								🟦			🟦
	1-Cyclohexene-1-methanol							🟩				
	1H-Imidazole-2-methanol		🟩			🟩						
	2(R),3(S)-1,2,3,4-Butanetetrol	🟦			🟦	🟦					🟦	
	2-Propanol, 1-chloro-3-propoxy-						🟦					
	2-Undecanol	🟩										
	3,5-Dithiahexanol 5,5-dioxide	🟦										
	3-Methyl-3-hexen-2-ol				🟩							
	4,5-Imidazoledimethanol			🟩								
	Cyclobutanemethanol	🟩					🟩					
	Cyclohexanol, 4-methyl-		🟩									
	Ethanol	🟥	🟥	🟥	🟥	🟥	🟥	🟥	🟥	🟥	🟥	🟥
	Ethanol, 2-bromo-					🟦						
	1-Penten-3-ol, 4-methyl-					🟩						
	2-Pentanol, 5-(2-propynyloxy)-							🟩				
	9-Methyl-Z-10-pentadecen-1-ol	🟩	🟦		🟦		🟦		🟦			
Acids	2-Butenoic acid, (E)-	🟩			🟩		🟩					🟩
	2-Hexynoic acid							🟩			🟩	

	2-Pentenoic acid							🟩				
	2-Pentenoic acid, 4,4-dimethyl-, methyl ester				🟩				🟩			
	2-Propenoic acid, 2-methyl-	🟩	🟩	🟩	🟩	🟩	🟩	🟩				
	3-Butenoic acid			🟩	🟩	🟩	🟩	🟩		🟩	🟩	🟩
	3-Pyridinecarboxylic acid, 4-hydroxy-				🟩							
	3-Pyrrolidin-2-yl-propionic acid	🟦							🟦			
	4-Oxopentanethioic acid									🟩		
	5,5-Dimethylbarbituric acid	🟦			🟦	🟦						
	5-Aminohexanoic acid									🟦	🟦	
	Acetic acid	🟥	🟥	🟥	🟥	🟥	🟥	🟥	🟥	🟥	🟥	🟥
	Acetic acid, 2-(N-methyl-N-phosphonatomethyl)amino-							🟩		🟩		
	Acetic acid, decyl ester		🟦									
	Acetoacetic acid, 1-thio-, S-allyl ester							🟩				
	Benzoic acid											🟩
	Butanoic acid, 2-diazo-3-oxo-, ethyl ester		🟦									
	Carbonic acid, 3-chlorophenyl neopentyl ester								🟦			
	Crotonic acid										🟩	
	Cyclobutanecarboxylic acid, oct-3-en-2-yl ester				🟩							
	Cyclopentaneacetic acid, ethenyl ester									🟩		
	Formic acid, 1-methylethyl ester				🟩							
	Guanidineacetic acid						🟩	🟩				🟩
	Hexanoic acid	🟩	🟩									
	Isocrotonic acid					🟩			🟩			
	Pentafluoropropionic acid, undecyl ester							🟩				

	Pentanoic acid, 3-methyl-		🟩									
	Pentanoic acid, 4-oxo-					🟩	🟩					
	Propanedioic acid			🟩	🟩	🟩						🟩
	Propanoic acid	🟩	🟩			🟩	🟩	🟩				
	Propanoic acid, 2-(aminooxy)-						🟩					
	Propanoic acid, 3-hydroxy-						🟩					
	1-Cyclopentene-1-carboxylic acid							🟩				
	2,3-Diazatetracyclo[3.3.0.0(4,7).0(6,8)]octane-3-carboxylic acid, methyl amide				🟩							
	4-Pentenoic acid, 2,4-dimethyl-, methyl ester						🟦					
	Bicyclo[2.2.2]octane-1-carboxylic acid		🟦						🟦			
	Cyclohexanecarboxylic acid, ethenyl ester								🟩		🟩	🟩
	Methoxyacetic acid, butyl ester							🟩				
	N-(2-Acetamido)iminodiacetic acid	🟦										
	.alpha.-Aminooxy-propionic acid, ethyl ester	🟩					🟩					
Ketones	1-(2-Isopropyl-5-methylcyclopentyl)ethanone							🟦				
	1,4-Dioxaspiro[5,5]undecan-3-one				🟩				🟩	🟩		
	2-Butanone, 4-hydroxy-3-methyl-	🟩				🟩		🟩				
	2-Butanone, diethylhydrazone			🟩	🟩							
	2-Cyclopenten-1-one, 2,3-dimethyl-			🟩								
	2-Cyclopenten-1-one, 2-methyl-								🟩			
	2-Hexanone, 6-	🟩										

	hydroxy-	🟩										
	2-Hydroxy-3,5,5-trimethyl-cyclohex-2-enone		🟦	🟦	🟦		🟦	🟦			🟦	🟦
	2-Propanone, 1-hydroxy-			🟩	🟩					🟩	🟩	
	6-Hydroxy-9-methyl-9-aza-bicyclo[3.3.1]nonan-3-one		🟦		🟦							
	6-Hydroxymethyl-5-methyl-bicyclo[3.1.0]hexan-2-one				🟦							
	Cyclohexanone		🟩			🟩						
	Cyclohexanone, 2-(hydroxymethyl)-				🟦							
	Cyclohexanone, 2-butyl-			🟩		🟩						
	Cyclohexanone, 3,3,5-trimethyl-			🟩	🟩							
	Cyclohexanone, 4-acetyl-							🟩				
	Cyclopentanone, 3-(3-hydroxy-1-propenyl)-				🟩							
	Cyclopentanone, 3-butyl-				🟩							
	Ethanone, 1-(3-pyridinyl)-					🟩						
	Ethanone, 1-(4-pyridinyl)-	🟩		🟩	🟩							
	6-Oxabicyclo[3.1.0]hexan-3-one, 2,2,4,4-tetramethyl-			🟦								
	1-Propanone, 1-cyclohexyl-						🟩					
	3-Buten-2-one, 4-(dimethylamino)-4-[(1-methylethyl)amino]-						🟦					
	3-Octen-2-one, 4-methoxy-			🟦								
	3-Pentanone, 1,5-dimethoxy-										🟦	
	Bicyclo[2.2.2]octanone, 4-methoxy-				🟩							
	Cyclopentanone, 2-methyl-				🟩							
	Hexahydro-1,4-dioxa-cyclopropa[a]p										🟩	

	entalen-3-one										🟩	
dione	1,3,5-Triazine-2,4(1H,3H)-dione, 6-(ethylamino)-				🟦							
	1,3-Cyclohexanedione, 5,5-dimethyl-					🟩						
	1,3-Dimethyl-3,4,5,6-tetrahydro-2(1H)-pyrimidinone			🟦								
	3,6-Diisopropylpiperazin-2,5-dione	🟦			🟦							
	4(1H)-Pyrimidinone, 2-amino-6-(methylamino)-			🟩								
	5,12-Naphthacenedione, 10-((3-(3-cyano-4-morpholinyl)-2,3,6-trideoxy-.alpha.-L-lyxo-hexopyranosyl)oxy)-7,8,9,10-tetrahydro-6,8,11-trihydroxy-8-(hydroxyacetyl)-1-methoxy-, (8S-cis)-		🟦									
	5-Methylhexane-2,4-dione, keto form	🟩										
	N-Ethylpiperazine-2,3-dione								🟩			
	Pyrrolo[1,2-a]pyrazine-1,4-dione, hexahydro-	🟦		🟦		🟦						
	Pyrrolo[1,2-a]pyrazine-1,4-dione, hexahydro-3-(2-methylpropyl)-	🟦	🟦			🟦		🟦	🟦	🟦		
	2,5-Piperazinedione, 3-methyl-6-(1-methylethyl)-	🟦				🟦						

Aldehydes	2-Hexenal, (E)-							🟩				
	2-Nonenal, (E)-			🟩	🟩							
	5-Thiazoleacetaldehyde, 4-methyl-			🟦								
	Benzaldehyde, 3-hydroxy-, oxime						🟦	🟦				
	Butalbital	🟦										
	Propanal, 3-methoxy-		🟩									
Flavones	Pyrrolidin-2-one, 5-[2-propionylethyl]-					🟩						
	2(1H)-Pyridinone	🟩		🟩				🟩				
	2,5-Dimethyl-4-hydroxy-3(2H)-furanone				🟩							
	2-Ethyl-1,3,4-trimethyl-3-pyrazolin-5-one		🟦									
	2-Furanone, 3,4-dihydroxytetrahydro											🟩
	2-Piperidinone		🟩		🟩							
	2-Pyrrolidinone	🟩	🟩	🟩	🟩	🟩	🟩	🟩	🟩	🟩	🟩	🟩
	2-Pyrrolidinone, 1-methyl-										🟩	🟩
	2-t-Butyl-1,3-dimethyl-imidazolidin-4-one		🟦									
	3,11-Diazabicyclo[4.4.1]undecan-4-one, 11-methyl-			🟦	🟦							
	3,4-Dihydroxy-5-methyl-dihydrofuran-2-one							🟩				
	5,6,7,8-Tetrahydro-thiazolo[5,4-c]azepin-4-one										🟦	
	5-Isopropylidene-3,3-dimethyl-dihydrofuran-2-one						🟦					

	6,7-Dihydro-2-methylamino-4H-oxazolo[3,2-a]-1,3,5-triazin-4-one		🟦					🟦				
	6-Methyl-3,5-heptadiene-2-one	🟩	🟩	🟩								
	Butyrolactone	🟩	🟩	🟩			🟩				🟩	
	Cycloheptano[d]imidazolidine, 1,3-dihydroxy-2-methyl-	🟩										
	Hydroquinone			🟦								
	3(2H)-Furanone, dihydro-5-methyl-		🟩									
	1,2-Dioxolan-3-one, 5-ethyl-5-methyl-4-methylene-			🟩								
	2(3H)-Furanone, 3-(dihydro-2(3H)-furanylidene)dihydro-				🟦							
	2,5-Methano-1H-inden-1-one, 2,3,3a,4,5,7a-hexahydro-			🟦								
	2-Allyl-3-thioxo-hexahydro-pyrrolo[1,2-c]imidazol-1-one										🟦	
	5,8-Decadien-2-one, 5,9-dimethyl-, (E)-								🟩			
	Octahydro-2H-pyrido(1,2-a)pyrimidin-2-one					🟦						
Flavonols	trans-1,10-Dimethyl-trans-9-decalol										🟩	
	4-Pyridinol				🟩						🟩	🟩
	D-Arabinitol								🟩			
	Diglycerol		🟦		🟦	🟦		🟦				
	DL-Arabinitol	🟩										
	dl-Threitol	🟩				🟦	🟦	🟦				
	Glycidol						🟩		🟩		🟩	
	L-Arabinitol						🟦					

	1,2,3,4-Butanetetrol, [S-(R*,R*)]-					🟦						
	Resorcinol						🟦					
	1,3-Benzodioxole, 2-methoxy-		🟦									
	2-Propyl-4-methylthiazole				🟦							
	4-Fluoroveratrole				🟦		🟦		🟦	🟦		🟦
	9H-Pyrido[3,4-b]indole		🟦	🟦	🟦	🟦						
	Isoxazole, 3,5-dimethyl-4-nitro-		🟦									
	Quinuclidine-3-ol						🟩					
	Thiazole, 2-butyl-4-methyl-											🟦
Phenols	Phenol	🟩	🟩	🟩	🟩	🟩	🟩	🟩	🟩	🟩	🟩	🟩
	Phenol, 2,6-dimethoxy-			🟩								
	Phenol, 2-ethoxy-			🟩								
	Phenol, 2-ethyl-			🟩								
	Phenol, 2-methoxy-	🟩	🟩	🟩	🟩	🟩	🟩	🟩	🟩	🟩	🟩	🟩
	Phenol, 2-methyl-			🟩								
	Phenol, 3,5-dimethoxy-			🟩		🟩						
	Phenol, 3-methyl-	🟩										🟩
	Phenol, 3-methyl-4-(methylthio)-										🟩	
	Phenol, 4-ethyl-					🟩	🟩	🟩	🟩	🟩	🟩	🟩
	Phenol, 4-ethyl-2-methoxy-									🟩		
	Benzeneethanol, 4-hydroxy-	🟥	🟥	🟥	🟥	🟥	🟥	🟥	🟥	🟥	🟥	🟥
	Benzenemethanol, 3-hydroxy-5-methoxy-		🟦						🟦			🟦
	Benzyl Alcohol		🟩		🟩	🟩						
	Benzyl alcohol, 4-fluoro-3-methoxy-					🟦						
	Homovanillyl alcohol	🟦	🟦	🟦	🟦	🟦	🟦	🟦	🟦	🟦	🟦	
	Phenylethyl Alcohol	🟩	🟩	🟩	🟩	🟩	🟩	🟩	🟩	🟩	🟩	🟩

Diols	1,2,3-Propanetriol, monoacetate		🟩									
	1,2-Benzenediol									🟩		
	1,2-Ethanediol, 1-(2-phenyl-1,3,2-dioxaborolan-4-yl)-, [S-(R*,R*)]-							🟦				
	1,3-Benzenediol, O-isobutyryl-O'-methoxyacetyl-									🟦		
	1H-Pyrido[2,3-b]indole						🟦					
	2-Ethyl-2-methyl-1,3-propanediol									🟦		
	2-Methyl-3-furanthiol	🟦		🟦	🟦							
	3-Pyrrolidinol								🟩			
	p-Dioxane-2,3-diol									🟩		
	1,2-Propanediol, 3-phenylthio-			🟦								
Dienes	1,2-Pentadiene			🟩								
	1,3-Nonadiene, (E)-											🟩
	1,3-Pentadiene, (Z)-		🟩									
	1,4-Hexadiene, 4-methyl-					🟩						
	1-Methoxy-1,4-cyclohexadiene		🟦									
acetate	1-Pentadecanol acetate									🟩		
	1-Tetradecyl acetate	🟩										
	6-Heptenyl acetate	🟩										
	Tricosyl acetate			🟩								
Glycols	Octaethylene glycol monododecyl ether	🟦	🟦	🟦	🟦	🟦	🟦	🟦	🟦	🟦	🟦	
	Glycerin	🟥	🟥	🟥	🟥	🟥	🟥	🟥	🟥	🟥	🟥	🟥
	Heptaethylene glycol monododecyl							🟦				

	ether							🟦				
	Thiodiglycol					🟦						
Nitriles	3-Pyrrolidinopropionitrile					🟦						
	3-Quinolinecarbonitrile				🟦							
	Butanenitrile, 4-(methylthio)-					🟩			🟩		🟩	🟩
	Hexadecanedinitrile		🟦									
	Undecanenitrile		🟦									
Amides	2,2-Dimethylcyclopropanecarboxamide										🟦	
	2-Butenediamide, (E)-							🟦				
	Acetamide					🟩						
	Acetamide, 2-fluoro-		🟩									
	Adipamide					🟦						
	Formamide, N,N-dimethyl-			🟩	🟩			🟩		🟩	🟩	🟩
	Hexanoic acid, 4-methylene-, methyl ester		🟦									
	l-Alanine ethylamide, (S)-								🟩	🟩		🟩
	Propionamide, 3-(1-piperidyl)-					🟦						
	Tetrahydropyrrole-3-amino-2,5-dione	🟩										
	Thiazole, 2-amino-5-methyl-					🟦						
Amines	1,2-Benzenediamine	🟩			🟩							
	1-Butanamine, 3-methyl-N-(3-methylbutyl)-N-nitroso-		🟦									
	1-Butanamine, N-methyl-								🟩			
	1-Pentanamine, N-methyl-										🟩	
	1-Propanamine, N,2-dimethyl-	🟩										

	2-Butanamine, (S)-								🟩			
	2-Butanamine, 3-methyl-			🟩	🟩							
	2-Pentanamine			🟩			🟩	🟩			🟩	
	2-Propanamine, 1-methoxy-						🟩					
	2-Propanamine, 2-methyl-N2-[1-tetrahydro-1H-1-pyrrolylmethylidene]											🟦
	2-Propen-1-amine, N,N-di-2-propenyl-			🟦			🟦					
	2-Pyridinamine, 3-methyl-		🟩							🟩		
	2-Pyridinamine, 5-methyl-			🟩		🟩						🟩
	4-Pyrrolidin-1-ylmethyl-thiazol-2-ylamine	🟦										
	Benzenamine, 4-methoxy-						🟩		🟩	🟩	🟩	
	Dimethylamine, N-(neopentyloxy)-					🟦				🟦		
	Ethanamine, N-ethyl-N-[(1-methylethoxy)methyl]-			🟩								
	Glycyl-l-glutamine						🟦					
	Isopropylamine hydrochloride								🟩			
	1-Methyl-1H-tetraazol-5-amine tbdms									🟦		
	1-Naphthalenecarbonitrile, 8-amino-				🟦	🟦						
	2-Pyridinemethanamine							🟩				
	4-Piperidinemethanamine						🟩					
	5-Methylthiophen-3-ylamine							🟦				
	Cyclopentanemethanamine, 5-amino-2,2,4-trimethyl-						🟦					
	N-Acetyltyramine		🟦									
	sec-Butylamine			🟩	🟩					🟩		

Alkanes	(E)-2-Butenylcyclopropane				🟩							
	1,2,3-Trimethyl-2-vinyl-1,3-diaza-2-silacyclopentane					🟦					🟦	
	1,2-Diazaspiro(2.5)octane	🟦	🟦									
	1,4,7,10,13,16-Hexaoxacyclooctadecane				🟦	🟦	🟦		🟦	🟦	🟦	
	1,9-Dioxa-4,12-diazadispiro[4.2.4.2]tetradecane, 3,3,11,11-tetramethyl-										🟦	
	1-Fluorononane			🟩								
	2-(2-Methyloxyryl)ethoxycarbonylmethoxyiminomethane								🟩			
	2-Methyl-3-vinyl-oxirane	🟩										
	3-Acetamido-3-ethyloctane								🟦			
	Cyclodecane, methyl-			🟦								
	Cycloheptane						🟩					
	Cyclohexane, 1,1'-ethylidenebis-									🟩		
	Cyclohexane, 1,4-dimethoxy-2-methyl-, stereoisomer									🟦		
	Cyclopropane, (2,2-dimethylpropylidene)-		🟦									
	Diallylmethylsilane		🟦									
	Oxirane, (methoxymethyl)-			🟩								
	Oxirane, trimethyl-	🟩										
	Propane, 1-chloro-3-(2-methoxyethoxy)-								🟩			
	1,3,2-Oxazaborinane, 2-butyl-	🟦										

	Ethane, 1-vinylthio-2-[(trimethylsilyloxy)ethylthio]-									🟦		
	Ethane, methoxy-			🟩								
	Heptane, 4-ethyl-					🟦						
Alkenes	2-Decene, (Z)-											🟩
	2-Decene, 3-methyl-, (Z)-					🟦		🟦				
	4-Cyanocyclohexene											🟩
	4-Decene					🟦						
	5-Decene								🟩			
	Benzene, 1-methoxy-2-(methylthio)-				🟦							
	Benzo[b]thiophene, octahydro-2-methyl-(2.alpha., 3a.alpha., 7a.alpha.)-						🟦			🟦		
	Cycloheptene		🟩	🟩								
	Thiophene, 2,5-dimethyl-			🟥								
	Thiophene, 3-methyl-										🟩	
Others	[2-(Diisopropylamino)ethyl]-(2-mercaptoethyl) sulfide	🟦										
	15-Crown-5						🟦		🟦			
	1H-Azepine, hexahydro-1-nitroso-										🟦	
	2,3,4,4a,8,8a-Hexahydro-pyrano[3,2-b]pyran		🟦									
	2,4-Diaminopyrimidine			🟩								
	2,5-Methano-2H-furo[3,2-b]pyran, hexahydro-		🟦									
	2,7-Dimethyl-3-oxo-5-methoxy-3,6(2H)-dihydro-1,2,4-triazepine				🟦							

	2-Acetoxy-N,N-dimethyl-2-propenamidine				🟦		🟦	🟦			🟦	
	2H-1-Benzothiopyran, octahydro-, trans-				🟦	🟦						
	2-Isopropylthiouracil									🟦		
	3,3-Dimethoxy-6,6-dimethyl-cyclohexa-1,4-diene		🟦	🟦								
	5-Isopropyl-3,3-dimethyl-2-methylene-2,3-dihydrofuran			🟩								
	Ala-gly, trimethylsilyl ester				🟩							
	Aziridine, 1-hexyl-				🟩							
	But-3-en-1-ynyl methyl sulfide										🟩	
	Carbon dioxide	🟩	🟩	🟩		🟩	🟩				🟩	🟩
	Chromyl chloride			🟦								
	Cyclohex-3-enecarboxaldehyde, 2,4,6-trimethyl-, oxime		🟦	🟦								
	Cytidine, 2'-deoxy-		🟦									
	D-Fructose, 1-O-methyl-				🟩							
	Diaziridine,3,3-dimethyl-					🟩						
	D-Serine	🟩										
	Furan, 2,4-dimethyl-			🟩								
	Furan, 2-methyl-5-(methylthio)-									🟦		
	Hydantoin, 1-butyl-								🟩			
	Hydrazine, N,N-dimethyl-N'-diethylboryl-					🟩						🟦
	Isosorbide Dinitrate	🟩										
	Isoxazolidine, 5-ethyl-2,4-dimethyl-, trans-				🟩							
	N-[2-[p-Methoxybenzyl]amino]ethylaziridine			🟦								

	N-[3-[.alpha.-Furylmethylamino]propyl]aziridine						🟦					
	N-[4-Aminobutyl]aziridine	🟦										
	Oxazolidine, 2-ethyl-	🟦										
	Oxazolidine, 2-methyl-2-propyl-									🟩		
	Piperazine, 1-methyl-				🟩							
	Piperidine, 1-methyl-		🟩									
	Pyridine, 3-ethyl-	🟩	🟩	🟩	🟩	🟩			🟩	🟩		
	Pyrrolidine, 1-(1-oxopentyl)-						🟦					
	Pyrrolidine, 2-(cyanomethylene)-				🟩							
	R(-)3,7-Dimethyl-1,6-octadiene		🟦									
	trans-2-Methyl-4-n-butylthiane, S,S-dioxide						🟦					
	water	🟥	🟥	🟥	🟥	🟥	🟥	🟥	🟥	🟥	🟥	🟥
	ammonia	🟥	🟥	🟥	🟥	🟥	🟥	🟥	🟥	🟥	🟥	🟥

APPENDIX B

Table 11: Appendix B

	Samples	**1.5 2h**	**1.5 4h**	**2.5 2h**	**2.5 4h**	**3.5 2h**	**3.5 4h**	**3.5 8h**	**5 2h**	**7 2h**	**9 2h**	**9 8h**
Alcohols	1-Pentanol, 2,3-dimethyl-					🟩			🟩			
	1-Pentanol, 2-ethyl-						🟩					
	1-Pentanol, 2-methyl-					🟩						
	1-Pentanol, 3-methyl-		🟥						🟩			
	1-Penten-3-ol, 2-methyl-			🟩								
	2-Furanmethanol, tetrahydro-, acetate							🟩			🟥	
	2-Hexanol				🟩							
	2-Hexen-1-ol, (Z)-	🟩										
	2-Hydroxymethylcyclopentanol (cis)		🟩		🟩		🟩					

	2-Hydroxymethylcyclopentanol (trans)			🟩								🟩
	2-Isopropyl-5-methyl-1-heptanol		🟩									
	3-Hexanol, 4,4-dimethyl-		🟩						🟩	🟩		
	Cyclohexanol							🟩				
	Cyclopentanol, 1-methyl-											🟩
	Cyclopentanol, 3-methyl-		🟩		🟩							
	Benzeneethanol, 4-hydroxy-		🟩			🟩						
	2-Penten-1-ol, acetate, (Z)-										🟩	
Acids / esters	.beta.-Alanine, N-methyl-, ethyl ester	🟩										
	1,2-Benzenedicarboxylic acid, bis(trimethylsilyl) ester							🟩			🟩	
	1,4-Benzenedicarboxylic acid, methyl trimethylsilyl ester							🟩				
	1H-Indole-2-carboxylic acid, 6-(4-ethoxyphenyl)-3-methyl-4-oxo-4,5,6,7-tetrahydro-, isopropyl ester		🟩								🟩	
	2-Chloroaniline-5-sulfonic acid						🟩					
	6-Tetradecanesulfonic acid, butyl ester					🟩	🟩					
	Carbonic acid, isobutyl isohexyl ester						🟩					
	Curan-17-oic acid, 2,16-didehydro-19-hydroxy-, methyl ester, (20.xi.)-											🟩
	Cyanic acid, propyl ester				🟥							
	Diglycolic acid				🟩							
	Formic acid, 1-(4,7-dihydro-2-methyl-7-oxopyrazolo[1,5-									🟩		

	a]pyrimidin-5-yl)-, methyl ester									🟩		
	Formic acid, chloro-, (3,4,4-trimethyl-1,2-dioxetan-3-yl)methyl ester					🟩						
	Fumaric acid, 2-decyl pentadecyl ester		🟩									
	Fumaric acid, cis-hex-3-enyl heptadecyl ester	🟩		🟩			🟩			🟩		
	Fumaric acid, dodecyl trans-hex-3-enyl ester											🟩
	Glycine, N-methyl-n-propoxycarbonyl-, tetradecyl ester									🟩		
	L-Alanine, ethyl ester											🟩
	L-Alanine, N-(N-acetylglycyl)-, butyl ester	🟩										
	l-Alanine, N-octanoyl-, hexadecyl ester			🟩								
	l-Alanine, N-octanoyl-, pentadecyl ester											🟩
	l-Alanine, N-propoxycarbonyl-, hexadecyl ester		🟩									
	l-Alanine, N-propoxycarbonyl-, hexyl ester										🟩	
	n-Capric acid isopropyl ester					🟩						
	n-Hexadecanoic acid					🟩						
	Nonanedioic acid, dihexyl ester						🟩					
	Oxalic acid, 2-ethylhexyl hexyl ester		🟩	🟩							🟩	
	Oxalic acid, 6-ethyloct-3-yl ethyl ester	🟩	🟩	🟩			🟩				🟩	
	Oxalic acid, allyl decyl ester			🟩						🟩		
	Oxalic acid, allyl pentadecyl ester											🟩
	Oxalic acid, bis(6-ethyloct-3-yl) ester											🟩
	Oxalic acid, cyclobutyl tridecyl ester		🟩									
	Oxalic acid,										🟩	

	cyclohexyl decyl ester										🟩	
	Oxalic acid, cyclohexyl dodecyl ester						🟩					
	Oxalic acid, dodecyl isohexyl ester			🟩								
	Oxalic acid, heptyl isohexyl ester											🟩
	Oxalic acid, hexyl isohexyl ester					🟩						
	Oxalic acid, hexyl propyl ester					🟩						
	Oxalic acid, isobutyl hexyl ester								🟩	🟩		
	Oxalic acid, isobutyl nonyl ester			🟩								
	Oxalic acid, isobutyl nonyl ester										🟩	
	Oxalic acid, isobutyl pentadecyl ester						🟩					
	Oxalic acid, isobutyl pentadecyl ester										🟩	
	Oxalic acid, isobutyl tetradecyl ester										🟩	
	Oxalic acid, monoamide, n-propyl, tridecyl ester							🟩				
	Oxalic acid, monoamide, n-propyl, undecyl ester	🟩		🟩								
	Oxalic acid, monomorpholide, nonyl ester					🟩						
	Pentafluoropropionic acid, decyl ester					🟩						
	Pentafluoropropionic acid, dodecyl ester							🟩				
	Pentafluoropropionic acid, hexadecyl ester					🟩						
	Sarcosine, N-isobutyryl-, tetradecyl ester						🟩		🟩	🟩		
	Succinic acid, heptyl tetrahydrofurfuryl ester		🟩	🟩			🟩	🟩	🟩	🟩		

	Sulfurous acid, 2-propyl tetradecyl ester		🟩									
	Sulfurous acid, 2-propyl tridecyl ester								🟩	🟩		
	Sulfurous acid, butyl dodecyl ester			🟩			🟩					
	Sulfurous acid, butyl heptadecyl ester				🟩							
	Sulfurous acid, butyl octadecyl ester										🟩	
	Sulfurous acid, butyl tetradecyl ester			🟩								
	Sulfurous acid, hexyl pentyl ester							🟩	🟩	🟩		🟩
	Sulfurous acid, nonyl 2-pentyl ester					🟩						
	Sulfurous acid, octadecyl 2-propyl ester					🟩						
	Thiazolidine-4-carboxylic acid, 2-(2-isopropoxyphenyl)-							🟩				
	Trichloroacetic acid, hexyl ester					🟩						
	Trifluoroacetic acid,n-tridecyl ester										🟩	
	2-Propenoic acid, 2-methyl-, 2-[[2,3,3a,4,7,7a(or 3a,4,5,6,7,7a)-hexahydro-4,7-methano-1H-indenyl]oxy]ethyl ester											🟩
	6-Tetradecanesulfonic acid, butyl ester					🟩	🟩					
	Butanoic acid, 3-oxo-, 2-propenyl ester					🟩						
	Carbonic acid, isobutyl isohexyl ester						🟩					
	Curan-17-oic acid, 2,16-didehydro-19-hydroxy-, methyl ester, (20.xi.)-											🟩
	Cyanic acid, propyl ester				🟥							

	Cyclohexane-1,3-dicarboxylic acid, 6-hydroxy-6-methyl-4-oxo-2-(2-phenylethenyl)-, diethyl ester							🟩				
	Dichloroacetic acid, hexyl ester					🟩						
	Nonahexacontanoic acid			🟩	🟩		🟩		🟩	🟩	🟩	🟩
	Propylphosphonic acid, di(2-ethylhexyl) ester					🟩						
	Tetrahydrofuran-2-carboxylic acid, dibenzofuran-3-ylamide				🟩			🟩				
	2-Propenoic acid, 2-methyl-, 2-methylpropyl ester					🟩		🟩				
	Cyclopentanecarboxylic acid, 2-tetrahydrofurylmethyl ester				🟩							
Ethers	1,2,3-Propatriol, 1-indol-4-yl(ether)							🟩				
	Methyl octyl ether					🟩						
	Pregnenolone, diisopropylsilyl ether		🟩									
Ketones	1-Propanone, 1-(1-cyclohexen-1-yl)-					🟩			🟩			
	2-Cyclohexen-1-one											🟩
	2-Cyclopenten-1-one, 2,3,4-trimethyl-		🟩									
	2-Cyclopenten-1-one, 2,3-dimethyl-	🟩	🟩	🟩	🟩	🟩			🟩			
	2-Cyclopenten-1-one, 2-methyl-	🟩	🟩	🟩		🟩						
	2-Heptanone, 4-methyl-	🟩						🟩	🟩		🟩	
	2-Hexanone	🟩	🟩	🟩	🟩	🟩	🟩	🟩	🟩	🟩	🟩	🟩
	2-Nonanone					🟩			🟩	🟥		
	2-Nonanone, 9-[(tetrahydro-2H-pyran-2-yl)oxy]-				🟩							
	2-Pentanone, 3-ethyl-		🟩									

	2-Pentanone, 4-hydroxy-4-methyl-					🟩						
	2-Propanone, methyl-2-propynylhydrazone											🟩
	3-Hexanone		🟩	🟩					🟩	🟩	🟩	
	3-Hexanone, 2-methyl-		🟩								🟩	
	3-Hexen-2-one					🟩	🟩					
	5-Hexen-2-one, 5-methyl-					🟩						
	Cyclohexanone	🟩			🟩	🟩						
	Cyclohexanone, 2,2,5,5-tetramethyl-3-methylene-										🟩	
	Cyclohexanone, 2-butyl-					🟩						
	Cyclohexanone, 2-pentyl-			🟩								
	Cyclohexanone, 2-propyl-		🟩									
	Cyclohexanone, 3-ethenyl-					🟩						
	Cyclohexanone, hydrazone			🟩								
	Ethanone, 1-(2-furanyl)-	🟩	🟩	🟩	🟩		🟩	🟩				🟩
	Ethanone, 1-(3-pyridinyl)-					🟩						
	Ethanone, 1-cyclopentyl-	🟩	🟩			🟩	🟩	🟩	🟩	🟩	🟩	
	Ethanone, 1-oxiranyl-					🟩						
	4-Penten-2-one, 4-methyl-					🟩						
Diones	2,3-Furandione, dihydro-4,4-dimethyl-	🟩										
	2,4-Hexanedione											🟩
	3,3-Dimethyl-2,4-pentane dione						🟩		🟩			
	3,5-Heptanedione, 2,2,4,6-tetramethyl-									🟩		
	1,2-Cyclohexanedione	🟩	🟩		🟩					🟩	🟩	
	2,5-Cyclohexadiene-1,4-dione, 2,6-bis(1,1-dimethylethyl)-								🟩	🟩	🟩	

Aldehydes	2-Hexenal, (E)-						🟩					
	2-Isopropyl-5-oxohexanal		🟩									
	3-Thiophenecarboxaldehyde		🟩			🟩						
	Benzal diacetate					🟩						
	Benzaldehyde	🟩		🟩								
	Benzaldehyde, 2-nitro-, diaminomethylidenhydrazone											🟩
	Benzaldehyde, 3,4-dimethyl-		🟩									
	Benzaldehyde, 3,5-dimethyl-			🟩				🟩	🟩	🟩	🟩	🟩
	Benzaldehyde, 4-propyl-				🟩							
	Benzeneacetaldehyde					🟩						
	Butanal, 4-[(tetrahydro-2H-pyran-2-yl)oxy]-										🟩	
	Hexanal				🟩							
	N,N-Dimethylformamide-di-t-butylacetal										🟩	
	Nonanal			🟩								
	Octadecanal		🟩									
	Pentadecanal-		🟩									
	Pentanal, 3-methyl-			🟩		🟩					🟩	
Flavones	1,1,4-Trimethyl-3-pyrazalone			🟩								
	1,2,3-Trimethylpiperidin-4-one	🟩										
	2(3H)-Furanone, 5-butyldihydro-4-methyl-, cis-				🟩							
	2(3H)-Furanone, dihydro-3-methyl-							🟩	🟩	🟩	🟩	🟩
	3(2H)-Furanone, dihydro-5-isopropyl-			🟩	🟩							
	5,6,7,8-Tetrahydro-thiazolo[5,4-c]azepin-4-one					🟩						
	5-Isopropylidene-3,3-dimethyl-dihydrofuran-2-one					🟩						

	3-(2-Ethyl-piperidin-1-ylmethyl)-8a-methyl-5-methylene-decahydro-naphtho[2,3-b]furan-2-one							🟩				
	3,6-Bis-dimethylaminomethyl-2,7-dihydroxy-fluoren-9-one	🟩						🟩				
	Di-n-decylsulfone							🟩				
	Butyrolactone					🟩						
Flavonols	1,1-Dodecanediol, diacetate					🟩						
	1,4-Pentadien-3-ol								🟩		🟩	🟩
	1H-1,2,4-Triazole, 3-methyl-		🟩						🟩			
	1-Hexacosanol			🟩								
	1H-Imidazole, 1-methyl-4-nitro-	🟩	🟩									
	1H-Indole, 3-methyl-		🟩									
	1H-Pyrrole, 2,3-dihydro-1-methyl-	🟩	🟩	🟩	🟩		🟩		🟩	🟩	🟩	🟩
	1H-Tetrazole					🟩						
	2,4-Pentadien-1-ol, 3-ethyl-, (2Z)-			🟩								
	2-Mercapto-4-phenylthiazole				🟩							
	3-Methyl-5-hydroxy-isoxazole				🟩							
Phenols	3,4-Dimethylbenzyl alcohol							🟩				
	Phenol	🟩	🟩	🟩	🟩	🟩	🟩	🟩	🟩	🟩	🟩	🟩
	Phenol, 2,4-bis(1,1-dimethylethyl)-	🟩	🟩	🟩	🟩	🟩	🟩	🟩	🟩	🟩	🟩	🟩
	Phenol, 2,4-bis(1-phenylethyl)-					🟩						
	Phenol, 2-methoxy-					🟩						
	Phenol, 2-propyl-		🟩									
	Phenol, 4,4'-(1-methylethylidene)bis-				🟩							

	Phenol, 4-ethyl-					🟩						
	Phenylethyl Alcohol		🟩			🟩						
	p-Isopropenylphenol				🟩							
	Cyclopropyl carbinol		🟩									
	Cyclopropyl methyl carbinol							🟥				
Dienes	1,15-Hexadecadiene										🟩	
	1,4-Pentadiene				🟩							
	1,6-Heptadiene									🟩	🟩	
	1,6-Heptadiene, 2,3,6-trimethyl-											🟩
	2-Oxabicyclo[3.2.0]hepta-3,6-diene					🟩						
	1,3-Pentadiene, 2-methyl-, (E)-										🟩	
Amine	(2,2-Dimethylcyclobutyl)methylamine			🟩		🟩						
	1,3-Propanediamine, N'-[3-(dimethylamino)propyl]-N,N-dimethyl-		🟩									
	1,3-Propanediamine, N-methyl-									🟩		
	1-Octadecanamine, N-methyl-			🟩								🟩
	1-Octanamine, N-methyl-						🟩					
	2-Anthracenamine										🟩	
	2-Butanamine, (S)-							🟩				
	2-Pentanamine	🟩							🟩	🟩		
	2-Pyridinamine, 4-methyl-					🟩			🟩			
	3,6-Acridinediamine, 2,7-dimethyl-							🟩				
	3-Hydroxy-N-methylphenethylamine	🟩										
	4,5,6-Pyrimidinetriamine		🟩									

	Borane, compd. with dimethylamine (1:1)	🟥										
	n-Hexylmethylamine	🟩		🟩								
	N-Trichloroacetyl-tryptamine										🟩	
	1,2,4-Triazol-4-amine, 5-ethyl-3-(3-methyl-5-phenylpyrazol-1-yl)-				🟩							
	2-Hexanamine, 4-methyl-	🟩										
Alkanes	(+)-2-Aminoheptane			🟩								
	[1,4,7]Trioxonane								🟩			🟩
	1,3-Dioxolane			🟩								
	10-Methylnonadecane			🟩	🟩		🟩				🟩	
	1-Bromoeicosane							🟩				
	1-Iodo-2-methylnonane	🟩					🟩					
	1-Iodo-2-methylundecane	🟩				🟩		🟩			🟩	
	1-Iodoundecane										🟩	🟩
	2,4-Dimethyldodecane	🟩			🟩		🟩					
	2,5-Dimethylhexane-2,5-dihydroperoxide					🟩						
	2,6-Dimethyldecane		🟩	🟩	🟩	🟩			🟩	🟩		
	2-Bromo dodecane	🟩	🟩						🟩			
	2-Bromotetradecane			🟩	🟩		🟩					🟩
	2-Cyclopropylcarbonyloxypentadecane											🟩
	Butane, 1-methoxy-2-methyl-								🟩	🟩		
	Butane, 2,2'-[methylenebis(oxy)]bis[2-methyl-			🟩								
	Butane, 2,2-dimethyl-											🟥
	Butane, 2-methyl-	🟥		🟥		🟥					🟥	🟥

	Cyclodecane, methyl-		🟩									
	Cyclododecane		🟩									
	Cycloheptane				🟩				🟩	🟩		
	Cyclohexane	🟩	🟩	🟩	🟩			🟩	🟩	🟩		🟩
	Cyclohexane, (1,3-dimethylbutyl)-						🟩		🟩	🟩	🟩	🟩
	Cyclohexane, (1-methylethyl)-	🟩	🟩	🟩					🟩	🟩	🟩	
	Cyclohexane, (1-methylpropyl)-							🟩				🟩
	Cyclohexane, (2-methylpropyl)-		🟩					🟩				
	Cyclohexane, (3-methylpentyl)-		🟩					🟩				🟩
	Cyclohexane, (4-methylpentyl)-						🟩					
	Cyclohexane, 1-(cyclohexylmethyl)-4-ethyl-, cis-								🟩	🟩		
	Cyclohexane, 1,1'-(1,3-propanediyl)bis-				🟩							
	Cyclohexane, 1,1'-(1,5-pentanediyl)bis-											🟩
	Cyclohexane, 1,1,3-trimethyl-	🟩						🟩				
	Cyclohexane, 1,1'-methylenebis-										🟩	
	Cyclohexane, 1,2,3-trimethyl-, (1.alpha.,2.beta.,3.alpha.)-						🟩					
	Cyclohexane, 1,2,4-trimethyl-		🟩			🟩						
	Cyclohexane, 1R-acetamido-2,3-cis-epoxy-4-trans-acetoxy-		🟩									
	Cyclohexane, butyl-								🟩	🟩		
	Cyclohexane, hexyl-		🟩									
	Cyclohexane, pentyl-										🟩	
	Cyclohexane, propyl-	🟩	🟩			🟩	🟩		🟩	🟩		
	Cyclooctane, butyl-								🟩		🟩	
	Cyclooctane, methyl-			🟩								
	Cyclooctane, methyl-							🟩				
	Cyclooctane, tetradecyl-			🟩								
	Cyclopentane, (2-methylpropyl)-	🟩	🟩									
	Cyclopentane,			🟩								

	1,1,3-trimethyl-			🟩								
	Cyclopentane, 1-ethyl-1-methyl-	🟩	🟩	🟩			🟩	🟩			🟩	🟩
	Cyclopentane, 1-ethyl-2-methyl-, cis-	🟩	🟩	🟩			🟩	🟩	🟩	🟩		🟩
	Cyclopentane, 1-ethyl-3-methyl-		🟩				🟩				🟩	
	Cyclopentane, 1-methyl-3-(1-methylethyl)-	🟩	🟩	🟩			🟩	🟩	🟩	🟩	🟩	🟩
	Cyclopentane, propyl-			🟩		🟩						
	Cyclopropane, 1-(1,2-dimethylpropyl)-1-methyl-2-nonyl-				🟩							
	Cyclopropane, 1-butyl-2-(2-methylpropyl)-							🟩				
	Cyclopropane, 1-ethyl-2-methyl-, cis-		🟥	🟩			🟩	🟩		🟩	🟩	
	Cyclopropane, 2-chloro-1,1,3-trimethyl-			🟩								
	Cyclopropane, propyl-			🟥		🟥						
	Decane	🟩	🟩	🟩	🟩		🟩	🟩	🟩	🟩	🟩	🟩
	Decane, 1,1'-oxybis-				🟩	🟩			🟩	🟩		🟩
	Decane, 1-iodo-	🟩						🟩				🟩
	Decane, 2,4,6-trimethyl-					🟩						
	Decane, 2-methyl-					🟩	🟩					
	Decane, 3,6-dimethyl-	🟩			🟩		🟩	🟩	🟩	🟩	🟩	🟩
	Decane, 3,7-dimethyl-	🟩	🟩	🟩		🟩	🟩	🟩	🟩	🟩	🟩	🟩
	Decane, 3,8-dimethyl-	🟩			🟩	🟩						
	Decane, 4-methyl-	🟩	🟩	🟩	🟩		🟩	🟩	🟩	🟩	🟩	🟩
	Decane, 5,6-dimethyl-	🟩	🟩	🟩		🟩	🟩	🟩	🟩	🟩	🟩	🟩
	Decane, 5-methyl-					🟩	🟩		🟩	🟩		🟩
	Docosane					🟩						
	Dodecane	🟥	🟥	🟥	🟥	🟥	🟥	🟥	🟥	🟥	🟥	
	Dodecane, 1-iodo-					🟩					🟩	
	Dodecane, 2,6,10-trimethyl-			🟩		🟩	🟩	🟩			🟩	
	Dodecane, 2,6,11-trimethyl-				🟩	🟩						
	Dodecane, 2-methyl-		🟩		🟩	🟩	🟩					
	Dodecane, 4,6-dimethyl-	🟩										

	Dodecane, 4-methyl-	🟩			🟩							
	Dodecane, 5,8-diethyl-										🟩	
	Eicosane	🟥	🟥	🟥	🟥	🟥	🟥	🟥	🟥	🟥	🟥	
	Eicosane, 10-methyl-	🟩			🟩							🟩
	Eicosane, 2,4-dimethyl-		🟩									
	Eicosane, 2-cyclohexyl-											🟩
	Eicosane, 9-octyl-							🟩			🟩	
	Heneicosane	🟥	🟥	🟥	🟥	🟥	🟥	🟥	🟥	🟥	🟥	🟥
	Heneicosane, 3-methyl-	🟩								🟩		
	Hentriacontane	🟥	🟥	🟥	🟥	🟥	🟥	🟥	🟥	🟥	🟥	🟥
	Heptacosane						🟩	🟩				🟩
	Heptadecane	🟩	🟩		🟩	🟩		🟩	🟩	🟩	🟩	
	Heptadecane, 2,6,10,15-tetramethyl-		🟩		🟩	🟩	🟩		🟩	🟩	🟩	
	Heptadecane, 2-methyl-					🟩	🟩		🟩	🟩	🟩	
	Heptadecane, 3-methyl-					🟩		🟩	🟩			
	Heptadecane, 4-methyl-					🟩						
	Heptadecane, 4-propyl-		🟩									
	Heptadecane, 8-methyl-				🟩	🟩						
	Heptadecane, 9-octyl-		🟩		🟩							
	Heptane						🟩	🟩	🟩	🟩		
	Heptane, 1-fluoro-										🟩	
	Heptane, 2,2,4,6,6-pentamethyl-				🟩							
	Heptane, 2,3-dimethyl-	🟩	🟩	🟩	🟩		🟩		🟩	🟩	🟩	
	Heptane, 2,4,6-trimethyl-			🟩				🟩			🟩	
	Heptane, 2,4-dimethyl-				🟩	🟩		🟩				🟩
	Heptane, 3-methyl-									🟩		🟩
	Heptane, 4,4-dimethyl-							🟩				
	Heptane, 4-ethyl-		🟩				🟩	🟩	🟩	🟩	🟩	
	Heptane, 4-methyl-	🟩										
	Hexacosane		🟩	🟩			🟩		🟩	🟩		
	Hexadecane	🟥	🟥	🟥	🟥	🟥	🟥	🟥	🟥	🟥	🟥	🟥
	Hexadecane, 1-iodo-						🟩					
	Hexadecane, 2,6,10,14-	🟩	🟩	🟩	🟩	🟩		🟩			🟩	

	tetramethyl-	🟩	🟩	🟩	🟩	🟩		🟩			🟩	
	Hexadecane, 2,6,11,15-tetramethyl-					🟩	🟩					
	Hexadecane, 2-methyl-					🟩	🟩		🟩	🟩	🟩	
	Hexadecane, 3-methyl-				🟩							
	Hexadecane, 7,9-dimethyl-					🟩						
	Hexadecane, 8-hexyl-8-pentyl-							🟩				
	Hexane	🟥	🟥	🟥	🟥	🟥	🟥	🟥	🟥	🟥	🟥	🟥
	Hexane, 1-fluoro-			🟥								
	Hexane, 2,3,4-trimethyl-			🟩	🟩							🟩
	Hexane, 2,3,5-trimethyl-		🟩		🟩		🟩	🟩	🟩	🟩	🟩	🟩
	Hexane, 2,3,5-trimethyl-						🟩					
	Hexane, 2,4-dimethyl-				🟩					🟩		
	Hexane, 2-methyl-						🟩					
	Hexane, 3-ethyl-										🟩	
	Hexane, 3-ethyl-2-methyl-									🟩		
	Hexane, 3-methyl-						🟩					🟩
	Isobutane	🟥	🟥	🟥			🟥	🟥	🟥	🟥		
	Nonadecane	🟥	🟥	🟥	🟥	🟥	🟥	🟥	🟥	🟥	🟥	🟥
	Nonadecane, 1-chloro-					🟩						
	Nonadecane, 2,3-dimethyl-					🟩	🟩					
	Nonadecane, 2-methyl-		🟩									
	Nonadecane, 3-methyl-				🟩							
	Nonadecane, 9-methyl-	🟩			🟩	🟩		🟩			🟩	
	Nonane	🟩	🟩					🟩			🟩	
	Nonane, 1-iodo-						🟩			🟩		
	Nonane, 2,5-dimethyl-	🟩	🟩	🟩	🟩		🟩	🟩	🟩		🟩	🟩
	Nonane, 2,6-dimethyl-					🟩	🟩					
	Nonane, 2-methyl-			🟩	🟩			🟩	🟩		🟩	🟩
	Nonane, 4,5-dimethyl-	🟩				🟩	🟩					
	Nonane, 4-ethyl-5-methyl-			🟩				🟩				
	Nonane, 5-methyl-											🟩
	n-Pentadecylcyclohexane					🟩						
	Octacosane	🟥	🟥	🟥	🟥	🟥	🟥	🟥	🟥	🟥	🟥	🟥

	Octadecane	🟥	🟥	🟥	🟥	🟥	🟥	🟥	🟥	🟥	🟥	
	Octadecane, 1-(ethenyloxy)-						🟩					
	Octadecane, 1-chloro-		🟩									
	Octadecane, 1-iodo-	🟩			🟩		🟩				🟩	
	Octadecane, 2,6-dimethyl-				🟩							
	Octadecane, 2-methyl-		🟩	🟩	🟩	🟩						
	Octadecane, 3-ethyl-5-(2-ethylbutyl)-	🟩	🟩	🟩			🟩	🟩	🟩			
	Octadecane, 3-methyl-				🟩			🟩	🟩			
	Octadecane, 5-methyl-						🟩	🟩	🟩		🟩	
	Octadecane, 9-ethyl-9-heptyl-				🟩							
	Octane										🟩	
	Octane, 1,1'-oxybis-	🟩										
	Octane, 2,2-dimethyl-		🟩									
	Octane, 2,3,3-trimethyl-								🟩	🟩		
	Octane, 2,4,6-trimethyl-					🟩						
	Octane, 2,6-dimethyl-					🟩						
	Octane, 2,7-dimethyl-				🟩							
	Octane, 2-bromo-		🟩									
	Octane, 2-cyclohexyl-						🟩					
	Octane, 2-methyl-					🟩					🟩	
	Octane, 3,4,5,6-tetramethyl-	🟩										
	Octane, 3,5-dimethyl-					🟩		🟩				🟩
	Octane, 3-ethyl-2,7-dimethyl-						🟩					🟩
	Octane, 4,5-diethyl-											🟩
	Octane, 4-ethyl-						🟩					
	Octane, 4-methyl-	🟩	🟩	🟩	🟩	🟩	🟩	🟩	🟩	🟩	🟩	🟩
	Octane, 5-ethyl-2-methyl-	🟩	🟩									
	Oxetane, 2,2,4-trimethyl-	🟩	🟩			🟩	🟩	🟩	🟩	🟩		
	Oxetane, 2,2-dimethyl-											🟩
	Oxetane, 2,3,4-trimethyl-, (2.alpha.,3.alpha.,4.beta.)-	🟩	🟩									
	Pentacosane	🟥	🟥	🟥	🟥	🟥	🟥	🟥	🟥	🟥	🟥	

	Pentadecane	🟥	🟥	🟥	🟥		🟥	🟥	🟥			
	Pentadecane, 2,6,10-trimethyl-			🟩	🟩							
	Pentadecane, 5-methyl-			🟩								
	Pentadecane, 8-heptyl-				🟩							
	Pentane, 2,2-dimethyl-							🟥				🟥
	Pentane, 2,3-dimethyl-	🟥	🟥	🟥				🟥	🟥	🟥	🟥	
	Pentane, 2,4-dimethyl-	🟩		🟩							🟩	🟩
	Pentane, 2-bromo-	🟥	🟥		🟥		🟥	🟥	🟥	🟥	🟥	🟥
	Pentane, 2-cyclopropyl-										🟥	
	Pentane, 2-methyl-				🟥			🟥	🟥		🟥	
	Pentane, 3-bromo-									🟩		
	Pentane, 3-methylene-				🟩							
	Tetracosane		🟩		🟩	🟩		🟩				🟩
	Tetracosane, 11-decyl-							🟩				
	Tetradecane	🟩		🟩	🟩	🟩	🟩	🟩	🟩	🟩	🟩	🟩
	Tetradecane, 2,6,10-trimethyl-				🟩			🟩				
	Tetradecane, 4-methyl-	🟩			🟩			🟩			🟩	
	Tetradecane, 5-methyl-		🟩								🟩	
	Tetrapentacontane, 1,54-dibromo-										🟩	
	Tetratetracontane			🟩	🟩							🟩
	Tetratriacontane	🟩	🟩	🟩	🟩	🟩	🟩	🟩	🟩	🟩	🟩	🟩
	Triacontane						🟩					
	Tridecane	🟩		🟩		🟩		🟩				
	Tridecane, 4-methyl-										🟩	
	Undecane		🟩				🟩					
	Undecane, 2,10-dimethyl-					🟩						
	Undecane, 2,6-dimethyl-				🟩	🟩		🟩	🟩			
	Undecane, 2-cyclohexyl-							🟩	🟩			
	Undecane, 2-methyl-				🟩	🟩				🟩		
	Undecane, 3-methyl-					🟩						
	Undecane, 4,4-dimethyl-						🟩					
	Undecane, 4,6-dimethyl-				🟩							
	Undecane, 4,8-dimethyl-	🟩										
	Undecane, 4-methyl-					🟩						

	Undecane, 5,7-dimethyl-											🟩
	Undecane, 5-methyl-	🟩						🟩	🟩			
	11-Methylnonacosane	🟩										
	1-Trifluoroacetoxy-2-methylpentane											🟩
	2,3-Dioxabicyclo[2.2.1]heptane, 1-methyl-					🟩						
	4-Trifluoroacetoxytridecane			🟩								
	Trifluoroacetoxyhexadecane						🟩					
Alkenes	17-Pentatriacontene				🟩							
	1-Docosene				🟩	🟩						
	1-Heptene	🟩		🟩	🟩						🟩	🟩
	1-Hexene			🟥	🟥		🟥					
	1-Hexene, 4-methyl-				🟩				🟩			
	1-Hexene, 5-methyl-											🟥
	1-Nonene			🟩				🟩	🟩		🟩	🟩
	1-Octene, 3,4-dimethyl-			🟩								
	1-Pentene, 2,3-dimethyl-											🟩
	1-Pentene, 2-methyl-	🟥	🟥	🟥	🟥	🟥	🟥	🟥	🟥	🟥	🟥	🟥
	1-Pentene, 4-methyl-		🟥	🟥	🟥		🟥	🟥	🟥	🟥	🟥	🟥
	1-Propene, 2-methyl-	🟩		🟥								
	1-Propene, 3,3'-oxybis-							🟩				
	2,3-Dimethyl-2-heptene						🟩					
	2,4-Dimethyl-1-heptene					🟩			🟩		🟩	
	2-Butene						🟩	🟩				
	2-Decene, 7-methyl-, (Z)-					🟩	🟩			🟩	🟩	
	2-Hexene, 3-methyl-, (Z)-						🟩		🟩			
	2-Pentene, 3-methyl-, (Z)-						🟩		🟩			
	3-Hexadecene, (Z)-								🟩	🟩	🟩	
	3-Hexene, (E)-					🟩		🟥				
	3-Hexene, (Z)-	🟥		🟥								
	3-Hexene,			🟩					🟩	🟩		🟩

	2,2,5,5-tetramethyl-, (Z)-			🟩					🟩	🟩		🟩
	3-Hexene, 2-methyl-, (E)-			🟩								
	4-Methyl-2-heptene	🟩										
	9-Eicosene, (E)-											🟩
	Cyclopentene											🟩
	Z-8-Hexadecene					🟩						
	(Z)-Hex-2-ene, 5-methyl-						🟩					
	2-Undecene, (Z)-										🟩	
	Toluene				🟩							
	Z-8-Hexadecene					🟩						
Alkynes	1-Nonyne						🟩	🟩				
	2-Hexyne			🟩								
Others	Acetone	🟥	🟥	🟥	🟥	🟥	🟥	🟥	🟥	🟥	🟥	🟥
	(+-)-cis-3,4-Dimethyl-2-phenyltetrahydro-1,4-thiazine				🟩							
	1,2-Bis(2-hydroxypropyl)hydrazine										🟩	
	1,6;2,3-Dianhydro-4-O-acetyl-.beta.-d-talopyranose					🟩						
	16-Hexadecanoyl hydrazide							🟩	🟩			
	1-Octadecanesulphonyl chloride					🟩						
	1-Pentyne, 3-ethoxy-3-ethyl-					🟩						
	2-[p-Methylphenyl]isatogen		🟩									
	2-Butoxyethyl acetate		🟩	🟩				🟩	🟩	🟩	🟩	
	2-Chloro-4-(4-methoxyphenyl)-6-(4-nitrophenyl)pyrimidine			🟩	🟩	🟩			🟩	🟩	🟩	
	2H-Pyran, 3,4-dihydro-6-methyl-		🟩			🟩						
	2H-Pyran-2-one, tetrahydro-6,6-dimethyl-										🟥	
	2-Hydrazino-4,6-dimethylpyrimidine ditms peak 2				🟩				🟩			

	2-Hydroxy-2-methyl-but-3-enyl 2-methyl-2(Z)-butenoate		🟩									
	2-Isobutylideneamino-3-methylbutyronitrile			🟩					🟩			
	2-Methyl-5,6,7,8-tetrahydroquinoxaline					🟩						
	2-Methylvaleroyl chloride											🟩
	3-Amino-2-phenazinol ditms							🟩				
	4-Chlorobenzenesulfonamide, N-methyl-			🟩								
	6-Methyl-3-heptyne					🟩						
	7-Amino-3-phenylcoumarin		🟩									
	7-Oxabicyclo[4.1.0]heptane, 2-methyl-		🟩				🟩					
	Ammonia				🟩	🟩						
	Aniline, N-methyl-					🟩						
	Aziridine, 2-methyl-2-(2,2,4,4-tetramethylpentyl)-					🟩						
	Azulene, 1,4-dimethyl-7-(1-methylethyl)-					🟩						
	Benzenamine, 3-fluoro-						🟩					
	Benzene, 1,2,3,4-tetramethyl-	🟩		🟩			🟩					
	Benzene, 1,2,3-trimethyl-							🟩				
	Benzene, 1,2,4,5-tetramethyl-	🟩	🟩			🟩			🟩	🟩	🟩	🟩
	Benzene, 1-ethyl-2,3-dimethyl-							🟩				
	Benzene, 1-methyl-2-(1-methylethyl)-						🟩				🟩	
	Benzene, 4-ethyl-1,2-dimethyl-			🟩				🟩	🟩	🟩		🟩
	Benzeneacetonitrile, .alpha.-hydroxy-							🟩				
	Bicyclo[2.2.2]octane-1-thiol, 4-methyl-					🟩						

	Butane, 1-isocyanato-							🟩				
	Caprolactam					🟩						
	Decyl trifluoroacetate					🟩						
	Didodecyl phthalate					🟩						
	Disulfide, di-tert-dodecyl					🟩						
	Erythro-dl-O-ethylthreonine	🟩										
	Formamide, N,N-dimethyl-	🟩			🟩							
	Furan, 2,5-dihydro-							🟩				
	Furan, tetrahydro-					🟩						
	Furan, tetrahydro-2,5-dimethyl-	🟩	🟩	🟩	🟩		🟩	🟩	🟩	🟩	🟩	🟩
	Furan, tetrahydro-2,5-dimethyl-, trans-(.+/-.)-				🟩							
	Furan, tetrahydro-2-methyl-			🟩								
	Hexahydropyrazin-1-propylamine, 4-[2-[3,4-dichlorophenyl]ethyl]-					🟩						
	Hexylene Glycol					🟥						
	Hydroperoxide, hexyl		🟩	🟩						🟩		
	Iminostilbene									🟩		
	i-Propyl tricosanoate			🟩		🟩						🟩
	l-Guanidinosuccinimide	🟩										
	l-Threitol, 2-O-nonyl-							🟩				
	l-Tyrophanamide							🟩				
	Meglumine										🟩	
	Methanaminium, 1-carboxy-N,N,N-trimethyl-, hydroxide, inner salt						🟩					🟩
	Methanimidamide, N,N-dimethyl-N'-[3-[[(methylamino)carbonyl]oxy]phenyl]-	🟩						🟩				🟩
	N-(Trifluoroacetyl)-N,O,O',O''-tetrakis(trimethylsilyl)norepinephr			🟩		🟩		🟩		🟩		

	ine			🟩		🟩		🟩		🟩		
	N-[4-(Acridin-9-ylamino)-phenyl]-acetamide							🟩				
	N-Benzyl-N-ethyl-p-isopropylbenzamide	🟩	🟩				🟩	🟩	🟩	🟩	🟩	🟩
	n-Hexanesulphonylacetonitrile	🟩	🟩	🟩		🟥		🟥			🟥	🟥
	Octacosyl trifluoroacetate									🟩		
	Oxazol-5(4H)-one, 4-(4-methoxybenzylideno)-2-(2,2-dimethylethyl)-										🟩	
	Oxime-, methoxy-phenyl-_				🟩							
	Oxirane, (2-methylbutyl)-										🟩	
	Oxirane, (3-methylbutyl)-		🟩	🟩							🟩	
	Oxirane, 2,2-dimethyl-3-propyl-					🟩	🟩					
	Oxirane, 2,3-diethyl-					🟩		🟩	🟩	🟩		
	Oxirane, 2-butyl-3-methyl-, cis-			🟩								
	Oxirane, 2-methyl-2-(1-methylethyl)-					🟩						
	Oxirane, 2-methyl-3-propyl-, cis-			🟩						🟩		
	Oxirane, 3-ethyl-2,2-dimethyl-							🟩				
	Oxirane, ethyl-				🟥					🟥		
	Oxirane, hexyl-				🟩							
	Oxirane, pentyl-						🟩	🟩	🟩			🟩
	Oxirane, tetramethyl-	🟩										
	Oxirane, tridecyl-									🟩		
	Pentanamide					🟥						
	Phosphetane, 2,2,3,4,4-pentamethyl-1-phenoxy-, 1-oxide							🟩				
	Piperazine, 2-methyl-	🟩										
	Piperazinetrione, [[2-(1,1-dimethyl-2-propenyl)-6-(3-					🟩						

	methyl-2-butenyl)-1H-indol-3-yl]methylene]-, (Z)-					🟩						
	Propanamide	🟩							🟩	🟩		
	Propane, 2-isocyano-2-methyl-			🟩								
	Pyrazine, 2,5-dimethyl-	🟩				🟩						
	Pyrazine, 2,6-dimethyl-					🟩						
	Pyrazine, 2-ethyl-3-methyl-	🟩										
	Pyrazine, 2-ethyl-5-methyl-					🟩						
	Pyrazine, 2-ethyl-6-methyl-	🟩										
	Pyrazine, methyl-					🟩						
	Pyrazolo[1,5-a]pyrimidine, 2,5,7-trimethyl-3-phenyl-							🟩				
	Pyrazolo[1,5-a]pyrimidine, 7-ethyl-5-methyl-2-phenyl-										🟩	
	Pyridine-3-carboxamide, oxime, N-(2-trifluoromethylphenyl)-		🟩			🟩						
	Pyrrolidine, 1-(2-(p-(3,4-dihydro-6-methoxy-2-phenyl-1-naphthyl)phenoxy)ethyl)-							🟩				
	Tetrahydropyran							🟩				
	Thieno[2,3-d]-1,3-thiaselenol-2-thione		🟩									
	Thiophene, 2,5-dimethyl-		🟩									
	Tocainide					🟩						
	trans-Crotonamide									🟩		
	Tridecanol, 2-ethyl-2-methyl-				🟩							

LEGEND

🟩	existing compounds with moderate peak height
🟥	existing compounds with high peak
🟦	existing long chain compounds eluting at the end